Summer 6-13-2014

Developing Crosslinking Constructs of Protein Kinase R

Prisma E. Lopez
University of Connecticut - Storrs, prismaelopez@gmail.com

Developing Crosslinking Constructs of Protein Kinase R

University of Connecticut
Honors Thesis
Prisma Lopez
Research Advisor: Dr. James L. Cole
Honors Advisor: Dr. Wolf-Dieter Reiter
Spring 2014

Acknowledgements

This thesis is an accomplishment I am proud of. I would like to thank all who have helped me through my undergraduate research journey and who taught me a thing or two about being a scientist. Firstly, I would like to thank Christopher B. Mayo for accepting to mentor me throughout my time in the Cole lab. Chris, I learned so much from you. Without your patience, knowledge, and kindness, I would not have grown as much as I did. I would also like to thank all current and past Cole lab members. Without your guys' suggestions research would have been a bit more tedious. I would also like to thank Dr. Wolf-Dieter Reiter for pointing out the important things about thesis writing. Lastly, I would like to give an enormous thanks to Dr. James L. Cole for taking me into his lab three years ago and for guiding me throughout the beginning of my life as a scientist.

Table of Contents

List of Figures

Abstract

Protein Kinase R (PKR) is a key component of the innate immune antiviral response. PKR is activated upon binding to dsRNA. However, recent studies have shown that PKR can also bind to and become activated by duplex RNAs containing complex secondary structure. The mechanism of PKR binding and activation by these RNAs is currently not known. The approach taken here to determine the mechanism of PKR binding by these RNAs is through the development of PKR constructs that are capable of covalently binding to RNAs. Constructs were created by site-specific incorporation of an unnatural, photoactivatable amino acid within PKR. These constructs were incubated with RNA and crosslinked at various UV light wavelengths. Subsequently, SDS-PAGE was performed to detect crosslinking products. The incentive for developing these crosslinking constructs is to use them to map PKR binding on RNAs and to determine the correlation between RNA structural features and PKR activation or inhibition.

Introduction

Protein Kinase R (PKR) is an enzyme involved in a multitude of cellular processes. Some of these critical processes are responses to stress signals such as cytokine responses, apoptosis, cell-growth, and pathogenic invasion (1-4). Although PKR is involved in a plethora of intracellular signaling pathways, we focus here on its role in the innate immune response.

Role of PKR in the Innate Immune Response

The innate immunity pathway is a non-adaptive defense mechanism that is activated by several pathogen-associated molecules. It is the initial response made by the body to eliminate pathogens and prevent disease (5). One protein involved in the human innate immune response is PKR. PKR is a cytoplasmic kinase that is induced by interferon as a response to pathogenic invasion (Figure 1) (6). PKR is composed of 551 amino acids and contains a C-terminal kinase domain connected to its N-terminal dsRNA-binding domain (dsRBD) by a 90 amino acid flexible linker (Figure 2). The protein becomes activated upon binding to dsRNA, a typical byproduct of viral replication (7). PKR binding to dsRNA occurs via its dsRBD, leading to activation of the kinase domain by autophosphorylation (8). Activated PKR then goes on to phosphorylate cellular substrates such as the alpha subunit of eukaryotic initiation factor (eIF2α), a protein involved in the initiation phase of translation (9). eIF2α's role is to mediate the binding of the initiator tRNA to the ribosome in a GTP-dependent manner; phosphorylation of eIF2α reduces protein synthesis by inhibiting initiation (10). Activation of PKR is crucial in that it inhibits translation and consequently, the replication of pathogens in infected cells.

PKR Structure

The critical structural domains of PKR are the catalytic kinase domain and the dsRBD. Upon activation, the kinase domain of PKR is autophosphorylated at multiple residues, including threonine 446 located in a flexible loop called the activation loop. Activated PKR than goes on to phosphorylate serine and threonine residues on substrates (11).

The other critical domain of PKR is the N-terminal dsRBD, which consists of two dsRNA-binding motifs, double-stranded RNA Binding Motif 1 (dsRBM1) and double-stranded RNA Binding Motif 2 (dsRBM2) (12). The dsRBD of PKR is among one of the many dsRBDs found in a multitude of proteins across various taxa (13). The dsRBD is a highly conserved structure that is typically 65-70 amino acids long (14). It contains a conserved α-β-β-β-α topology, in which the N- and C- terminal α-helices pack against one face of a three-stranded antiparallel β-sheet (15). The domain is present in proteins implicated in many aspects of cellular life, from RNA editing, RNA processing, RNA transport, RNA silencing, and antiviral response as is the case with PKR.

The successful activation of PKR is attributed to the binding of the protein's dsRBD to dsRNA in a sequence independent manner (16). In addition, the dsRBD is highly specific for dsRNA with little or no observable binding to ssRNA, dsDNA, or ssDNA; the size and shape of the grooves confers specificity for dsRNA over dsDNA (17). The sequence independent characteristic of the dsRBD is due to the limited interaction with the bases on dsRNA (18). Structural studies of dsRBDs indicate that protein-RNA contacts are mediated through aromatic and basic residues, mostly located throughout looped regions within the domain (19-20). Mutational analyses of various different dsRBDs have demonstrated the importance of the highly conserved α-helix at the C-

terminal end of the domain for the interaction with RNA. The basic amino acids within this α-helical region contact the RNA (21).

PKR Activation Model

PKR is potently activated by dsRNAs upon binding via the dsRBD. The most well accepted structural model for PKR activation suggests that PKR exists in an open conformation whereby dimerization of PKR is necessary for autophosphorylation and activation (Figure 3) (22). This model is supported by the observation that dimerization of PKR can initiate autophosphorylation reactions in the absence of dsRNA (23). Inactive PKR exists primarily as a monomer but can dimerize weakly, with a dissociation constant of 500 μM. In the presence of dsRNA, autophosphorylation rates are greatly increased and the population of PKR dimers is enhanced because it is thought that dsRNA serves as a scaffold for PKR dimerization. Therefore, in the presence of dsRNA, the population of PKR molecules forming dimers is increased resulting in greater autophosphorylation activity. A characteristic feature of PKR autophosphorylation is the bell shaped curve of activation where small concentrations of dsRNA activate but higher concentrations inhibit the protein (24). The current interpretation is that low concentrations of dsRNAs favor the assembly of PKR dimers on a single dsRNA whereas high concentrations of dsRNA cause PKR monomers to separate onto different molecules of dsRNA (25-26).

Interaction of PKR with RNA

In vitro activation studies have revealed that a dsRNA of 85bp is the optimal length for PKR activation and that a dsRNA of 30bp is the minimum length requirement for binding and activation (27). A minimum dsRNA length requirement suggests that the RNA must be long enough to accommodate two PKR monomers. PKR interactions with RNAs in the cell are not limited to perfect duplexes. Some of these RNAs contain complex secondary structures such as stem-loops and bulges, with single- and double-stranded regions. It is believed that the secondary structures of various RNAs that interact with PKR determine the RNA's ability to induce either PKR activation or inhibition. As an example, one study showed PKR activation to be induced by a 16 bp stem loop RNA containing ~10 nucleotide ssRNA tails at the 5' and 3' ends (ss-dsRNA) (28). Most notable about this RNA activator is that its structure deviates substantially from the typical structural requirements needed to activate PKR. Although the dsRNA stem loop of the 16 bp ss-dsRNA contains less than the minimal length (30 bp) required to activate PKR, the ss-dsRNA still activates the protein. Activation of PKR by this ss-dsRNA suggests that the tails, by means not yet understood, contribute to PKR activation.

The Cole lab is working to define where PKR binds to ss-dsRNAs as well as determining their mechanism of PKR activation. Our studies are based on a model ss-dsRNA : 15-15-15. The nomenclature for these RNAs is as follows: the first and last numbers represent the length of the 5' and 3' arms, respectively. The center number represents length of the double stranded stem. Modifications to this RNA have been accomplished and have involved symmetrically and asymmetrically shortening the 5' and 3' single-stranded-regions. It has been determined that the ss-regions of the 15-15-

15 RNA are required for PKR activation; deletion of either region abolishes the ability for PKR to become activated (Mayo and Cole, unpublished results). This observation suggests that the single-stranded regions are somehow interacting with PKR to induce activation.

In addition, PKR interactions with more complex inhibiting RNAs have been documented (29). One such RNA is Adenovirus Virus-Associated RNA I (VAI). Human cell infection by adenovirus results in the production of VAI which function to evade the immune response. VAI is a potent inhibitor of PKR that binds but fails to activate the protein (30). Inactivation of PKR by VAI is accomplished by tight binding of only a single monomer of PKR (31). The sequestering of a PKR monomer by VAI inhibits dimerization and therefore activation of PKR. Inactivation of PKR results in the continued replication of the virus within the host cell. It is believed that the secondary and tertiary structural features of VAI contribute to the high affinity binding of PKR to VAI.

It remains unclear as to how the structural features of inhibitory RNAs, such as VAI, and activating RNAs, such as ss-dsRNAs, contribute to either inhibition or activation of PKR (Figure 4). A method for determining the localized binding of PKR to RNA ligands is necessary in order to reveal how the binding of PKR to specific RNA structural features result in either the activation or inhibition of PKR.

Developing a Crosslinking Construct of PKR

Motivation

The approach taken here to determine the binding of PKR on structurally complex RNAs is to create a functional crosslinking construct of PKR. The construct would

ideally covalently bind to RNAs of interest *in vitro* upon UV irradiation. Successful development of these constructs would be useful to map the RNA structural regions PKR binds on activating or inactivating RNAs, such as ss-dsRNAs and VAI, respectively.

A Method for Creating Crosslinking Constructs of PKR

Many techniques for identifying and characterizing protein-nucleic acid interactions have been described. One such technique requires the incorporation of an unnatural amino acid with photo-crosslinking capabilities into the protein of interest (32).

Photo-crosslinkers have been used extensively as probes to identify and map interactions between proteins and DNA or RNA molecules. Proteins of interest with incorporated photo-crosslinkers enable the protein to selectively form covalent complexes with their cognate DNA or RNA binding site upon UV irradiation. The crosslinking occurs upon sample exposure to UV light, whereby a reactive radical forms and in turn creates a covalent bond to proximal atoms. The benefit of this approach is that it is possible to gain insight into the interaction interface between the biological macromolecules because it is possible to control the placement of the crosslinker.

The unnatural amino acid chosen for site-specific incorporation into PKR at dsRBM1 for this study was p-azido-L-phenylalanine (pAzF) (Figure 5). This unnatural amino acid was chosen because of the reactive chemistry of the azide functional group upon UV exposure. Upon UV radiation, the three doubly bonded nitrogens of the azide group participate in a reaction where a reactive radical is formed thereby rapidly inducing a covalent interaction with adjacent atoms. In addition, pAzF was the chosen unnatural amino acid because it is cost-effective.

Expanding the Cell's Biosynthetic Machinery

In order to successfully incorporate the unnatural amino acid, it was necessary to add new components of the protein biosynthetic machinery into the *Escherichia coli (E. coli)* expression system used here. A method for incorporating unnatural amino acids into *E. coli* and *Saccharomyces cerevisiae (S. cerevisiae)* has been developed and was employed here (33).

To site-specifically incorporate the unnatural amino acid into PKR, a single codon that corresponds to the candidate amino acid residue for pAzF substitution was mutated to the amber stop codon TAG. This was a critical step in the development of the constructs, as the codon coding for the unnatural amino acid must not code for any of the other endogenous amino acids. The TAG amber stop codon was used since it is the least used among the three stop codons in *E. coli* and because it has been shown to rarely terminate the synthesis of critical proteins.

As pAzF is not found normally within cells, it was necessary to introduce an orthogonal tRNA-aminoacyl-tRNA synthetase pair that could specifically incorporate pAzF into PKR in response to the TAG stop codon. Here, the orthogonal tRNA–synthetase pair used was derived from a tyrosyl-tRNA synthetase pair from the archaeon *Methanococcus jannaschii* (34). Archaeal tRNAs have distinct aminoacyl-tRNA synthetase recognition elements relative to *E. coli*, and therefore do not cross-react with the endogenous synthetases of *E. coli*, this offers an advantage to using the pair in *E. coli*. The tyrosyl-tRNA synthetase pair is expressed at high levels and in a functional form in *E. coli*. The pair has consequently been used to incorporate a growing number of unnatural amino acids into proteins in *E. coli* (35). pAzF has been

successfully incorporated into other proteins and was shown to be efficiently translated by the amber suppressor tRNA *in vivo* and *in vitro* (36).

Design of PKR Constructs

Each construct had the single pAzF incorporated within dsRBM1 of PKR. dsRBM1 was selected for mutational analysis to test the potential of the method to map PKR's localized binding on dsRNAs. The development of the constructs here is a pilot project to design and create other functional crosslinking constructs of PKR in different regions. These other regions on PKR include dsRBM2 and the kinase domain. These efforts are being made in order to determine where PKR is binding on certain structural features that in turn either activate or inactivate the protein.

In order to determine the amino acid residues on dsRBM1 that would be appropriate for pAzF incorporation, we aligned the dsRBD sequences of PKR, *Drosophila* Staufen protein, *Xenopus laevis* RNA-binding protein A-2 (Xlrbpa-2), *E. coli* RNAs III, and human TAR-RNA binding protein. The alignment was performed to determine which residues were highly conserved. The residues that were conserved among the five proteins were then eliminated from the pool of candidate amino acids because their conservation across proteins from different species suggests them to be of structural or functional importance.

Subsequently, the crystal structure of Xlrbpa-2 complexed with dsRNA was used as a basis for selecting target PKR residues because there is no structure of the PKR dsRBD bound to dsRNA (Figure 6) (37). The NMR structure of PKR dsRBD was overlayed with the crystal structure of Xlrbpa-2 using PYMOL. Residues were selected on the basis of their proximity to the RNA and on their sequence homology (Figure 7).

The structural homology between the dsRBD of Xlrbpa and the dsRBD of PKR readily allowed determination of candidate amino acid targets. The amino acid residues selected for substitution were F9, F43, D38, R39, N65, and E29 on PKR. Of these, we successfully substituted pAzF in place of F9, F43, E29, and D38. These constructs are designated F9pAzF, F43pAzF, E29pAzF, and D38pAzF respectively.

Materials and Methods

Plasmid selection

The PKR gene and the lambda phosphatase gene were inserted into the pET-11a plasmid used here. In this modified pET-11a plasmid, the lambda phosphatase gene is downstream the PKR gene which is under the T7 promoter. Site-directed mutagenesis was performed on this modified plasmid to create PKR construct plasmids containing the site-specifically incorporated TAG amber stop codon. The pEVOL plasmid, which contained the *M. jannaschii* orthogonal *tRNA-aminoacyl tRNA synthetase pair* gene was used to transform the *E. coli* expression system used here along with the modified pET-11a PKR construct plasmid.

Site-directed Mutagenesis

The forward and reverse primers used for the site directed mutagenesis were ordered from IDT and each contained the TAG mutation at the sequence corresponding to a candidate amino acid (Figure 8). In each 50 μL PCR reaction mixture, primers were at a concentration of 0.2 μM with the template at a concentration of 10.4 ng/μL. Site-directed mutagenesis was carried out under the following conditions using the Phusion HF polymerase purchased from New England BioLabs:

1. 95°C for 2 min
2. 95°C for 30 sec
3. 62°C for 30 sec
4. 72°C for 4 min
5. Go To step 2, 30-times
6. 72°C for 5 min
7. 4°C Hold

Following the PCR reaction, 1 μL of DpnI (20,000units/mL) was added to each 50 μL PCR reaction and incubated for one hour at 47°C prior to transforming cells with the desired mutated plasmid.

Arctic Express Competent Cells from Agilent Technologies was the chosen cell line for transformation for antibiotic resistance screening purposes. 100 μL of Arctic Express Cells were thawed on ice and mixed gently for five minutes. The cells were then transformed with the mutated pET-11a and pEVOL plasmid. Both the pEVOL and pET-11a plasmid (25ng/μL) were added to the cell mixture to a final concentration of 50ng/μL. The cells were subsequently incubated on ice for 30 minutes and then heat pulsed in a 42°C water bath for 20 seconds. Next, the cells were transferred to an ice bucket for a 2-minute incubation period. 900 μL of warm SOC media was added to the transformation reaction and the sample was then incubated at 37°C for 1 hour with shaking at 250 rpm. 100 μL of transformed cells were grown on LB agar plates containing carbenicillin and chloramphenicol to select for the pET-11a and pEVOL plasmid, respectively. The plates were then incubated for 18 hours at 37°C.

Large-Scale Protein Expression

To prepare for large-scale protein expression, 10 mL aliquots of sterile LB containing chloramphenicol and carbenicillin were inoculated with a single colony from

the growth plate. The 10 mL cultures were incubated at 37°C with shaking at 250 rpm for 18 hours. Following growth, two 2 L flasks containing LB Broth without antibiotics were each inoculated with 10 mL of overnight culture and incubated at 37°C. Cell growth was monitored by collecting 1 mL of cell culture sample and measuring the absorbance of the sample at 600 nm. When the absorbance of the cell sample reached approximately 0.2, 500 μL of Arabinose (20%) was added along with 1 mL of pAzF solution (0.5 M in 1 M NaOH). Arabinose was added in order to induce expression of the tRNA-aminoacyl synthetase pair gene. Once the absorbance of the cell sample reached approximately 1, the cell cultures were cold-shocked for 15 minutes at 4°C and 1 mL of pre-induction samples were collected. After cold shocking, the cultures were induced with 500 μL of 1 M IPTG. The cell cultures were then allowed to incubate at 37°C until the samples reached an absorbance close to 2. 1 mL post-induction samples were collected for SDS-PAGE analysis. The 500 mL cultures were then spun down at 8,500 rpm for 10 minutes and the cell pellet was saved for protein purification at -80°C.

Prior to thawing the post-induction cell pellets, 400 μL of Sigma Protease Inhibitor Cocktail per liter of cell culture was added to the pellet. After thawing, the pellet was suspended in 8.3 mL of Buffer A.

Buffer A: 20 mM HEPES, pH 7.5
50 mM NaCl
0.1 mM EDTA
10% Glycerol

Cell lysis was accomplished by sonication using the Fisher Scientific Sonic Dismembrator Model 100 sonication machine. The cell sample was sonicated for 40 seconds six times at the 8th setting on ice. In between each 40-second interval the sonicator was turned off. Following sonication, the sample was centrifuged at 22000 *g*

for 20 minutes and the supernatant was saved. The pellet was then suspended in 5 mL Buffer A and sonicated again as above. The cell sample was then re-centrifuged for 22000 *g* for 20 minutes and the supernatant was collected. Supernatant samples from the first and second centrifugation were then pooled and centrifuged one last time.

Protein Purification

For each 1 L prep, a single 5 mL HiTrap Heparin HP column was used. The column was first washed with Buffer A prior to run for a volume of 50mL at a flow rate of 2.5 mL/min. Subsequently, to remove any excess material on the column that was flown through it previously, the column was washed with 13% of Buffer B until the OD was done to a baseline flow rate.

Buffer B: 20 mM Hepes, pH 7.5
1.2 M NaCl
0.1 mM EDTA
10% Glycerol

The supernatant acquired from the cell-lysis purification step was loaded onto the Heparin column at 2.5 mL/min. Then, Buffer B was used to elute the protein from the heparin column. 20% of Buffer B was initially used to elute the protein. Increasing the percentage of Buffer B used by 5% increments until the percent of Buffer B used to elute the protein was 80% subsequently eluted the rest of the protein sample. The PKR construct containing fractions were then stored at 4°C overnight. Due to time constraints, no further purification of the constructs was performed.

Prior to using each protein sample in a crosslinking reaction, the absorbance of each sample at 280 nm was determined. As each protein sample was not entirely pure, five absorbance readings at 280 nm were taken and the average of the five

absorbances was calculated. The mean absorbance value was used to determine the approximate concentration of the PKR construct in the heterogeneous protein sample. The Beer-lambert law was employed in calculating the concentration of PKR construct using the extinction coefficient of PKR ε=43341.9 $M^{-1}cm^{-1}$.

Labeling with a Fluorescent Fluorophore

In order to verify the incorporation of pAzF in each construct, the Heparin purified protein samples were reacted via click chemistry with an Alexafluor® 488-conjugate containing a strained alkyne reactive group. 250 μL of each protein sample was incubated with 2.0 μL of the fluorophore conjugate (10 mM) for one hour. Following the one-hour incubation period, the protein sample was buffer exchanged into AU75 buffer.

AU75 Buffer: 20 mM Hepes, pH 7.5
75 mM NaCl
0.1 mM EDTA

Prior to the exchange, 2.5 mL of 1x P6 Biogel beads were added to a 15 mL falcon tube and centrifuged for four minutes at 1000 rpm to separate the beads from the TE Buffer. The supernatant was then removed and 5 mL of AU75 Buffer was added to the tube, mixed, and centrifuged for 4 minutes at 1000 rpm. This was repeated three more times and following each centrifugation, the supernatant was removed. For the fifth centrifugation step, a Pierce Centrifuge column was placed into the 15 mL falcon tube and the AU75 buffer-bead mix was transferred to the column and centrifuged again. The flow through was then disposed. After the last centrifugation with AU75, a new 15 mL collection tube was used and the 250 μL labeled sample was loaded into the column

containing the beads and centrifuged at 1000rpm for four minutes. The buffer-exchange protein sample was then collected for analysis

The absorbance of the protein sample at 488 nm was then determined using the Thermo Scientific NanoDrop 2000. Successful incorporation of the unnatural amino acid is indicated by an absorbance peak at 488 nm in the spectrum due to the Alexa Fluor absorbance.

Crosslinking

For the crosslinking studies, the 115 VAC UV lamp from Cole Palmer was used to crosslink samples at 254 nm, 302 nm, or 365 nm. A 96-well plate was used to hold the samples and the samples were placed on ice during the entire crosslinking procedure. The UV lamp was held approximately 2 cm from the 96-well plate.

Each purified PKR construct was crosslinked in the presence of a 45 bp duplex RNA or a 15-15-15 RNA at wavelengths of 254 nm, 302 nm, or 365 nm. Wild type PKR (WT PKR) was also crosslinked at 254, 302, and 365 nm with either type of RNA as a control. In each 20 μL crosslinking reaction, the final concentration of RNA and protein was 1 μM and 4 μM respectively. Au75 was the buffer used in each reaction and enough of the buffer was added to reach a final volume of 20 μL. 20 μL of UV exposed samples were collected following exposure over the course of 1, 2, 5, 10, and 30 minute(s).

In addition, both WT PKR and the PKR constructs were exposed to UV light at 254 nm, 302 nm, or 365 nm in the absence of RNA. Samples were collected at the same time points as mentioned above. Lastly, samples at the same six time points were collected for WT PKR and the PKR constructs incubated with either RNA type that was not exposed to UV light.

45bp duplex RNAs purchased from Dharmacon were prepared by annealing the complementary top (88 μM) and bottom strands (84 μM). For the annealing procedure, the RNAs were incubated together at equimolar concentrations of 20 μM and heated in a heat block at 90°C for five minutes. Following heating, the samples were allowed to cool in the heat block on a bench top until the temperature of the samples reached room temperature. The annealed samples were then stored in 7 μL aliquots at -80°C.

The 15-15-15 RNA samples were prepared by diluting the stock sample (197 μM) to 2 μM in AU75 buffer. The RNA sample was than annealed after diluting by heating the sample to 90°C for five minutes and then by plunging it into ice for ten minutes. 100 μL aliquots were then stored at -80°C.

Gel Electrophoresis

12% Resolving and 4% stacking SDS-PAGE gels for this experiment were prepared according to the Bio-Rad SDS-PAGE preparation protocol. In all cases, the running buffer used was 1X Tris-glycine. The gels were run at 200 V and 500 mA for 50 minutes. In all gels, 5x gel loading buffer was added to gel samples to 20% (v/v). BME was not added to the 5X loading gel buffer prior to loading to avoid reducing the azide group on the unnatural amino acid. The gel-loading buffer was prepared as shown below.

5X Gel Loading Buffer: 312.5 mM Tris-HCl
10% SDS
50% Glycerol
0.005% Bromophenol Blue
5 mM EDTA

Results

The sequencing results for four out of the six construct plasmids showed successful incorporation of the TAG codon in the appropriate location (data not shown). Problems with the PCR did not allow for successful substitution of the TAG amber stop codon at the appropriate positions to make N65pAzF and R39pAzF construct plasmids.

As indicated by SDS-PAGE, all post-induction cell lysate samples showed no significant amounts of PKR construct present where both inducers were added (Figure 9-10). However, the presence of lambda phosphatase (λ PP) is suggested in the cell lysate samples containing IPTG. λ PP is approximately 25kDa in size and prominent bands appear between the 26kDa and 19kDa markers in the cell lysates containing IPTG (Figure 9-10). The presence of this protein was not verified by western blotting. λ PP kept the PKR constructs in their unphosphorylated form.

Despite the minimal presence of PKR constructs in the post-induction samples, large-scale protein expression was pursued followed by purification by Heparin column to determine if it was the case that really small amounts of each PKR construct were being produced by the *E. coli* cells used here rather than none.

As indicated by SDS-PAGE of the fractions, PKR construct was present. Bands close to the WT PKR band are found across all construct samples purified by Heparin column (Figure 11-14). The fractions selected for pooling were typically fractions 24, 25, or 26 up to fraction 32 for the F43pAzF, D38pAzF, and E29pAzF constructs purified (Figure 11-13). However, for the F9pAzF construct, fractions 36—44 were pooled (Figure 14). The pooling strategy was such that only fractions containing minimal amounts of contaminant protein were pooled. Of great importance was to eliminate as much of the

protein that appears immediately below the PKR band as shown by SDS-PAGE. Further purification was not accomplished due to time constraints.

Following the labeling of each PKR construct with Alexa488 and buffer exchange into AU75, the absorption spectrum of each partially purified protein sample was recorded. It was assumed that the fluorescently labeled heterogeneous protein sample contained mostly labeled PKR construct and minimal amounts of labeled endogenous *E. coli* protein. Additionally, it was assumed that only a negligible amount of endogenous *E. coli* protein had incorporated pAzF because the amber stop codon is rarely used in *E. coli*. As indicated by the spectra, the fluorophore was successfully incorporated into the following constructs: F43pAzF, D38pAzF, and E29pAzF (Figure 15-17). The fluorophore was not successfully incorporated into F9pAzF and the spectrum is not shown here. WT PKR was labeled with the flurophore as a control (Figure 18). As can be seen in the absorption spectra for each successfully labeled construct, an absorbance peak is observed at 488nm in addition to absorbance peaks at 230nm and 280nm. An absorbance peak at 488nm suggests successful pAzF incorporation because the fluorophore in coordination with the azide group on pAzF absorbs light at this wavelength. For WT PKR, the peak at 488nm is not observed since it does not contain the unnatural amino acid.

Crosslinking at 254nm of WT PKR in the absence of RNA resulted in significant cross-linked product formation over a 30-minute time course (Data not shown). Cross-linked product formation was also observed in the crosslinking reaction of WT PKR in the presence of a 40bp RNA or a 15-15-15 RNA at 254nm over time (Data not shown). Crosslinking of WT PKR at 302nm in the absence of RNA or the presence of either a 45bp RNA or a 15-15-15 RNA also resulted in the formation of cross-linked products

near the top of the gel except in smaller amounts compared to the crosslinking reactions done at 254nm (Figure 19).

Crosslinking of the F43pAzF mutant at a wavelength of 254nm also resulted in crosslinked product formation in the absence of RNA and in the presence of either 45bp RNA or a 10-15-15 RNA (Figure 20). Subsequent crosslinking experiments were not performed with this mutant due to limited availability. Crosslinked products also formed in the absence and presence of RNA with the E29pAzF construct upon 302nm UV light exposure (Figure 21). Crosslinking at 254nm with this construct was not performed because protein-protein products are inevitable under these conditions.

Since protein-protein and protein-RNA crosslinked products were inevitably forming upon sample exposure to 254nm or 302nm wavelengths of light, subsequent crosslinking reactions with the remaining PKR constructs were performed at a wavelength of light of 365nm.

As revealed by SDS-PAGE, crosslinking of WT PKR in the absence or presence of RNA at 365nm resulted in no crosslinked product formation over a 30-minute time course (Figure 22). This was a desirable outcome for the project because it eliminated non-specific crosslinking.

SDS-PAGE shows no crosslinked product formed as a result of crosslinking the E29pAzF or D38pAzF construct in the absence of RNA at 365nm over time (Figure 23—24). Crosslinking of D38pAzF to a 15-15-15 ss-dsRNA or to a 45bp dsRNA over time shows no convincing crosslinked product formation over time (Figure 25). In addition, no convincing crosslinked product is formed as a result of E29pAzF crosslinking with a 45bp dsRNA or to a 15-15-15 ss-dsRNA under the same conditions (Figure 26). In either case, very minor banding occurs at the top of the gel at the 30-minute time point but it is

not significant. This banding could be background material and not crosslinked product. Western blotting could have been performed to verify that the bands are crosslinked products that contained the constructs and not of any other endogenous *E. coli* proteins as well.

Discussion

Throughout the course of this project, several challenges were faced. The first was obtaining adequate levels of each PKR construct. PKR construct induction tests revealed no observable amounts of PKR construct in the cell lysate samples induced with IPTG and arabinose. Large-scale protein expression was still pursued followed by purification by Heparin column to determine if it was the case that the Arctic Express cell line was producing minimal amounts of the protein rather than none. SDS-PAGE of the fractions pooled for each construct purified by Heparin suggested the presence of the respective constructs. This suggested than that minimal amounts of PKR construct were being produced within the cells used here. Low levels of PKR construct were not considered to be due to low levels of pAzF in the growth media. The concentration of pAzF added here is considered appropriate and sufficient. Increasing the amount of pAzF in the growth media is not encouraged in the literature because increasing the concentration of pAzF in the media results in decreased cell growth rates (data not shown). For the purposes of obtaining sufficient PKR construct for the crosslinking reactions, more cells were grown.

It remains a puzzle as to why PKR construct production was low in our *E.coli* cells. The high levels of λ PP in the cell lysate samples containing IPTG indicate that IPTG was inducing expression of the PKR construct gene and the λ PP gene since the two protein coding genes are in sequence with one another and are both under the T7

promoter. Presumably the PKR construct and λ PP coding mRNA transcript is being produced and high levels of λ PP are being translated and maintained in the cells but minimal levels of PKR construct are being produced. Low levels of PKR construct could be because incorporation of pAzF into the growing peptide chain is not efficient; that the tRNA is not very effective at recognizing the amber stop codon. Alternatively, the Arctic Express Cells are recognizing the amber stop codon and producing truncated PKR construct products and small amounts of full-length construct. pAzF incorporation at different positions within the Aha1 protein of *S. cerevisiae* also showed strong suppression of the amber stop codon for each variant (38). These explanations are just educated assumptions and by no means are sufficient alone to explain what is occurring intracellularly. Studies to determine the mechanisms responsible for low PKR construct production were not performed here.

After large-scale protein expression, purification by Heparin column was achieved followed by labeling of each partially purified construct-containing sample. Labeling each PKR construct protein was key because it was necessary to verify that pAzF was successfully incorporated into the protein prior to using it in crosslinking studies. While the absorption spectra of each partially purified PKR construct sample showed incorporation of the fluorophore, it does not suggest that only the PKR construct had pAzF incorporated into it. The probability exists that at least some *E. coli* proteins contained pAzF if any other endogenous mRNA transcripts also contained the UAG amber stop codon. However, it was assumed here that a negligible amount of endogenous *E. coli* proteins contained pAzF because the amber stop codon UAG is rarely used in E. coli (39). Only 7% of the *E. coli* protein coding genome contains an amber stop codon. Had any of these endogenous *E. coli* proteins contributed to the

crosslinking observed in any of the crosslinking experiments performed here, their contribution was assumed to be negligible.

After successful labeling, samples with either construct in the absence and presence of RNA were exposed to UV light of different wavelengths to induce crosslinking. Samples containing WT PKR with or without RNA were also exposed to different wavelengths of UV light. This was done to verify that crosslinking upon UV light exposure was specific to the constructs only in the presence of RNA.

We found that inducing crosslinking with UV light at 365nm was appropriate for PKR construct-RNA binding studies. Wavelengths shorter than 365nm (254nm and 302nm) were deemed inappropriate for PKR construct-RNA binding studies because they induced crosslinking in samples containing WT PKR or PKR construct in the absence and presence of RNA. The formation of cross-linked products with WT PKR was not expected because WT PKR does not contain the photoreactive unnatural amino acid pAzF. Additionally, crosslinking was only expected to occur between constructs that contained pAzF in the presence of RNA.

Recently it was shown that it is possible to induce covalent crosslinks in biologically relevant peptides upon short and medium UV wavelength irradiation. However, only peptides containing aromatic side chains generate crosslinked products upon exposure to UV light, demonstrating that the crosslinking reaction requires the presence of aromatic amino acids (40). The aromatic amino acids tryptophan, tyrosine, and phenylalanine absorb UV light and are highly susceptible to oxidation by one or more reactive oxygen species (ROS) generated following UV light exposure (41). Upon absorption of UV light, the aromatic side chains produce ROS such as •OH or $O_2^{-\bullet}$, which consequently react readily to generate covalent bonds with neighboring residues

or other molecules (42-44). Presumably, the aromatic side chains within WT PKR are mediating the crosslinking between the proteins to itself upon 254nm or 302nm UV light exposure. The same could be occurring between the constructs crosslinked here at short and medium wavelengths.

In addition, UV induced protein-nucleic acid crosslinking has been well documented (45-47). In particular, extensive protein-nucleic acid crosslinking occurs following UV light exposure within the 220nm-290nm range. Presumably the aromatic residues in the constructs and WT PKR are mediating the crosslinking of the protein(s) to RNA following short and medium wavelength exposure. Crosslinked products presumably do not form upon 365nm UV light wavelength exposure because this wavelength is outside the optimal electromagnetic absorption range of the aromatic residues (48). Non-crosslinking of WT PKR at 365nm was encouraging because it suggested crosslinking with the PKR constructs could be performed at this wavelength without having background non-specific (WT PKR) crosslinking occurring as well.

Once crosslinking was determined to be appropriate at 365nm of light, crosslinking experiments were performed with two PKR constructs in the presence and absence of RNA. Crosslinking of the E29pAzF or D38pAzF construct in the absence of RNA resulted in no crosslinked product formation. A qualitative analysis of the SDS-PAGE results for E29pAzF or D38pAzF crosslinking to RNA suggest no significant or convincing amount of crosslinked product formed over time. The insignificant decrease in band intensity of each non-crosslinked PKR construct over time also supports this.

By qualitative analysis alone, it is not readily discernible whether the minor banding appearing at the top of the gel at the 30-minute time point in the SDS-PAGE of the D38pAzF crosslinked sample with a 45bp dsRNA and the E29pAzF with either RNA

type is certainly protein-RNA crosslinked product. The banding may just be background material. Verification of the identity of the banding could have been performed by western blotting or with more sensitive methods. If indeed the crosslinked products formed contained either construct, further experiments could be performed to determine how to optimize the amount of crosslinked product formed. Verification would also be necessary to show that the crosslinked products predominantly contained the pAzF incorporated PKR constructs rather than any other pAzF incorporated endogenous *E. coli* protein(s).

Perhaps crosslinking is occurring but at really low levels which SDS-PAGE cannot resolve. Crosslinked product formation could be supported by either the appearance of bands towards the top of the gel over time, or by the decrease in intensity of the uncrosslinked PKR construct band over time. The crosslinking experiments performed with E29pAzF or D38pAzF do not suggest either to be the case. Perhaps the decrease in the non-crosslinked band intensity is minimal and reflects the formation of crosslinked product at the top of the gel. However, we cannot be certain of this until studies to verify this have been performed.

It was expected that had crosslinking occurred between any construct and RNA, PKR construct crosslinking would be more prominent with a 45bp dsRNA than to a 15-15-15 ss-dsRNA. The reasoning behind this is because the binding event of the second PKR monomer on a 40bp dsRNA is 52.5nM [Kd_2] in Au75 (49), whereas the binding event of the second PKR monomer on a 15-15-15 ss-dsRNA is 294nM in AU75 (Cole and Mayo unpublished results). It was assumed that the dissociation constant of two PKR monomers on a 45bp dsRNA is comparable to the 40bp dsRNA case although this has not been demonstrated. Presumably crosslinking would have more readily occurred

between more tightly bound PKR construct—RNA ligands assuming the incorporation of pAzF into PKR did not perturb PKR construct binding to RNA ligands or affinity for them.

Autophosphorylation assays and binding assays were not performed here to verify that incorporation of pAzF did not significantly alter the protein's activation or affinity for RNA. If pAzF did affect the structure of E29pAzF or D38pAzF, it could have affected its affinity for RNA and consequently this could have affected the crosslinking reaction.

Future Directions

Overall, the crosslinking studies performed here at 365nm of UV light with E29pAzF or D38pAzF are not sufficient to suggest the functionality of either construct as a potential tool for PKR-RNA mapping studies. In the future, very pure protein samples of any of the four constructs made here should be crosslinked to RNA to eliminate crosslinking of *E. coli* pAzF-incorporated proteins to RNA. Prior to this however, autophosphorylation and gel-shift assays should be performed to verify that pAzF incorporation did not affect PKR activation or binding to RNA. A comparative analysis of the crosslinked products that result from the crosslinking could yield insight into which construct is preferable for crosslinking studies. Presumably, the construct that yields the most crosslinked product would be the preferred one to use in PKR-RNA mapping studies.

If crosslinking of either construct at 365nm results in similar results obtained here, the position of pAzF can be substituted to make new constructs. One reason a small amount of cross-linked product maybe forming is because the RNA backbone is

not readily accessible to the azide group in the construct. The azide group within the crosslinker must make close enough contact with the RNA backbone so that upon UV irradiation, covalent interaction of the azide group of pAzF to the RNA can readily occur. Crosslinked product yield has been shown to depend on the location of pAzF into the protein of interest (38). Perhaps the location of pAzF on some of the constructs made here is not ideal and is causing low crosslinked product yield. For future projects the crosslinker could be placed at other regions on PKR for optimization purposes.

Alternatively, pAzF could be substituted with a different unnatural amino acid that is photoactivateable at long wavelengths. Crosslinking studies have been performed in the past using the unnatural amino acid p-benzoyl-phenylalanine (pBpa) (50). pBpa has been used extensively to characterize protein-protein interactions and protein-DNA interactions (51-53).

The use of pBpa as the preferred photoreactive group for photoaffinity crosslinking experiments is because of the following. The benzophenone group in pBpa is chemically more stable than alternative photoreactive groups such as diazo esters, aryl azides, or diazarines (54). pBpa's wavelength range of activation (350nm-360nm) causes no harmful effects to protein and it preferentially covalently binds to C-H atoms (55). Also and most importantly, unlike other photoreactive groups, the excitation of benzophenone to a ROS diradical triplet stage is reversible. Upon excitation with UV light, if there is no interacting partner available in close proximity, the benzophenone group undergoes many chemical cycles until a preferable geometry for covalent modification is achieved (56). This property, combined with an optimal lifetime of the excited state, results in efficient covalent modifications of macromolecules, usually with high site specificity. In addition, benzophenone groups react minimally with water. This

is unlike the case for aryl azides where if no interacting partner is available in close vicinity, the group reacts with water (57). For the purposes of this study, it is highly desirable to use a photocrosslinker that is able to covalently bind site-specifically and to relevant molecules. pBpa is potentially a better candidate for site-specific incorporation into PKR than pAzF is because the wavelength needed to activate the benzophenone group on pBpa is long enough to avoid background non-specific crosslinking. In the future, incorporation of pBpa into PKR could be tried to see if its properties in effect allow for greater site-specific crosslinked product to form.

Alternatively, groups with unique chemistry such as a specific metal chelator could be attached to the azide group on pAzF within the PKR constructs already made here to identify the binding sites of dsRBM1 on RNA ligands by affinity cleavage. Upon interaction with RNA, the metal chelator within the protein would induce cleavage of the RNA at the interaction interface. The affinity cleavage approach has been performed previously and led to the identification of binding sites for the individual dsRMBs on various RNA ligands including VAI (58). Similarly, the affinity cleavage approach could be employed here to characterize the binding sites of PKR to RNAs of the ss-dsRNA type and many others.

References

1) Nakamura, T., Furuhashi, M., Li, P., Cao, H., Tuncman, G., Sonenberg, N., Cem, Z.G., and Hotamisligli, G.S. (2010) Double-Stranded RNA-Dependent Protein Kinase Links Pathogen Sensing with Stress and Metabolic Homeostasis. Cell. 140, 338-348.

2) Kapil, P., Stohlman, S.A., Hinton, D.R., and Bergmann, C.C. (2014) PKR mediated regulation of inflammation and IL-10 during viral encephalomyelitis. J Neuroimmunol. 270, 1-12.

3) Zhang, P., Li, Y., He, J., Pu, J., Xie, J., Wu, S., Feng, L., Huang, X., and Zhang, P. (2014) IPS-1 plays an essential role in stress granule formation induced by dsRNA through interacting with PKR and mediating its activation. J. Cell. Sci. [Epub ahead of print]

4) Jagus, R., Bhavesh, J., and Barber, G.N. (1999) PKR, apoptosis and cancer. Int. J. Biochem. Cell. Biol. 31, 123-138.

5) Murphy, Kenneth, Paul Travers, Mark Walport, and Charles Janeway. *Janeway's Immunobiology*. New York: Garland Science, 2011.

6) Toth, A. M., Zhang, P., Das, S., George, C. X., and Samuel, C. E. (2006) Interferon action and the double-stranded RNA-dependent enzymes ADAR1 adenosine deaminase and PKR protein kinase. Prog. Nucleic Acid Res. Mol. Biol. 81, 369-434.

7) Robertson, H.D., and Matthews, M.B. (1996) The regulation of the protein kinase PKR by RNA. Biochimie. 78, 909-914.

8) Roman, P.R., Garcia-Barrio, M.T., Zhang, X., Wang, Q., Taylor, D.R., Zhang, F., Herring, C., Matthews, M.B., Qin, J., and Hinnebusch, A.G. (1998) Autophosphorylation in the activation loop is required for full kinase activity in vivo of human and yeast eukaryotic initiation factor 2 alpha kinases PKR and GCN2. Mol. Cell. Biol. 18, 2282-2297.

9) P.J. Farrell, K. Balkow, T. Hunt, R.J. Jackson, and H. Trachsel (1977) Phosphorylation of initiation factor elF-2 and the control of reticulocyte protein synthesis. Cell. 11, 187–200.

10) Kimball, S.R. (1999) Eukaryotic initiation factors eIf2a. IJBCB. 31, 25-59.

11) Garcia, M.A., Meurs, E.F., and Esteban, M. (2007) The dsRNA protein Kinase PKR: Virus and Cell control. Biochimie. 89, 799-811.

12) Tian, B., Bevilacqua, P. C., Diegelman-Parente, A., and Mathews, M. B. (2004) The double-stranded-RNA-binding motif: Interference and much more. Nat. Rev. Mol. Cell Biol. 5, 1013–1023.

13) St Johnston,D., Brown, N.H., Gall,J.G. and Jantsch, M. (1992) A conserved double stranded RNA-binding domain. Proc. Natl Acad. Sci. USA. 89, 10979–10983.

14) Masliah, G., Barraud, P., and Allain, F.H.T. (2013) RNA recognition by double-stranded RNA binding domains: a matter of shape and sequence. Cell. Mol. Life. Sci. 70, 1875-1895.

15) Nanduri, S., Carpick, B. W., Yang, Y., Williams, B. R., and Qin, J. (1998) Structure of the double-stranded RNA binding domain of the protein kinase PKR reveals the molecular basis of its dsRNA-mediated activation. EMBO J. 17, 5458–5465.

16) Ryter, J. M., and Schultz, S. C. (1998) Molecular basis of double- stranded RNA-protein interactions: Structure of a dsRNA-binding domain complexed with dsRNA. EMBO J. 17, 7505–7513.

17) Bass, B.L., Hurst, S.R., and Singer, J.D. (1994) Binding properties of newly identified Xenopus proteins containing dsRNA-binding motifs. Cell. 4, 301-314.

18) Steitz, T.A. (1993) The RNA World (Gestland R.F., Atkins, J.F., eds), pp. 219-237, Cold Sprig Harbor Laboratory, Cold Spring Harbor, NY.

19) Bycroft, M., Grunert, S., Murzin, A.G., Proctor, M., and Johnston, D. S. (1995) NMR solution structure of a dsRNA binding domain from Drosophila staufen protein reveals homology to the N-terminal domain of ribosomal protein S5. EMBO. 14, 3563-3571.

20) Kharrat, A., Macias, M.J., Gibson, T.J., Nilges, M., and Pastore, A. (1995) Structure of the dsRNA binding domain of E. coli RNase III. EMBO. 14, 3572-3584.

21) McCormack, S.J., Thomis, D.C., and Samuel, C.E. (1992) Mechanism of interferon action: identification of a RNA binding domain within the N-terminal region of the human RNA-dependent P1/eiF-2 alpha protein kinase. Virology. 188, 47-56.

22) Heinicke, L. A., Wong, J., Lary, J., Nallagatla, S.R., Diegelman-Parente, A., Zheng, X., Cole, J.L., and Bevilacqua, P.C. (2009) RNA Dimerization promotes PKR dimerization and activation. J. Mol. Biol. 390, 319-338.

23) Lemaire P.A., Lary, J., and Cole, J.L. (2005) Mechanism of PKR activation: dimerization and kinase activation in the absence of double-stranded RNA. J. Mol. Biol. 345, 81-90.

24) Hunter, T., Hunt, T., Jackson, R.J., and Robertson, H.D. (1975) The characteristic of inhibition of protein synthesis by double-stranded ribonucleic acid in reticulocyte lysates. J. Biol. Chem. 250, 409-417.

25) Kostura, M., and Mathews, M.B. (1989) Purification and Activation of the double-stranded RNA-dependent eIF-2 kinase DAI. Mol. Cell. Biol. 9, 1576-1586.

26) Zhang, F., Romano, P.R., Nagamura-Inoue, T., Tian, B., Dever, T.E., Mathews, M.B., Ozato, K., and Hinnebusch, A.G. (2001). Binding of double-stranded RNA to protein kinase PKR is required for dimerization and promotes critical autophosphorylation events in the activation loop. J. Biol. Chem. 276, 24946–24958.

27) Manche, L., Green, S.R., Schmedt, C., and Mathews, M.B. (1992) Interactions between double-stranded RNA regulators and the protein kinase DAI. Mol. Cell. Biol. 12, 5238-5248.

28) Zheng, X., and Bevilacqua, P.C. (2004) Activation of the protein kinase PKR by short double-stranded RNAs with single-stranded tails. RNA. 10, 1934-1945.

29) Langland, J. O., Cameron, J. M., Heck, M. C., Jancovich, J. K., and Jacobs, B. L. (2006) Inhibition of PKR by RNA and DNA viruses. Virus Res. 119, 100–110.

30) Ghadge, G.D., Malhotra, P., Furtado, M.R., Dhar, R., and Thimmapaya, B. (1994) In vitro analysis of virus-associated RNA I (VAI RNA): inhibition of the double-stranded RNA-activated protein kinase PKR by VAI RNA mutants correlates with the in vivo phenotype and the structural integrity of the central domain. J. Virol. 68, 4137-4151.

31) Kitajewski, J., Schneider, B., Munemitsu, C.E., Samuel, C.E., and Thimmappaya, B. (1986) Adenovirus VAI RNA antagonizes the antiviral action of interferon by preventing activation of the interferon-induced eIF-2 alpha kinase. Cell. 45, 195-200.

32) Chin, J.W., and Schultz, P.G. (2002) In vivo photocrosslinking with unnatural amino acid mutagenesis. Chembiochem. 3, 1135-1137.

33) Wang, L., and Schultz, P.G. (2006) Expanding the genetic code. Annu. Rev. Biophys. Biomol. Struct. 35, 225-249.

34) Wang, L., Magliery, T.J., Liu, D.R., and Schultz, P.G. (2000) A New Functional Suppressor tRNA/Aminoacyl-tRNA Synthetase Pair for the in Vivo Incorporation of Unnatural Amino Acids into Proteins. J. Am. Chem. Soc. 122, 5010-5011.

35) Xie, J., and Schultz, P.G. (2006) A chemical toolkit for proteins. Nature. 7, 775-782.

36) Chin, J.W., Santoro, S.W., Martin, A.B., King, D.S., Wang, L., and Schultz, P.G. (2002) Addition of p-Azido-l-phenylalanine to the Genetic Code of Escherichia coli. J. Am. Chem. Soc. 124, 9026-9027.

37) Nanduri, S., Carpick, B.W., Yang, Y., Williams, B.R.G., and Qin, J. (1998) Structure of the double-stranded RNA-binding domain of the protein kinase PKR reveals the molecular basis of its dsRNA-mediated activation. EMBO. 18, 5458-
5465.

38) Berg, M., Michalowski, A., Palzer, S., Rupp, S., and Sohn, K. (2014) An In Vivo Photo-Cross-Linking Approach Reveals a Homodimerization Domain of Aha1 in S. cerevisiae. PLOS. 9, 1-9.

39) Nakamura, Y., Gojobori, T., and Ikemura, T. (2000) Codon usage tabulated from international DNA sequence databases: status for the year 2000. Nucl. Acids. Res. 28, 292.

40) Leo, G., Altucci, C., Bourgoin-Voillard, Gravagnulo, A.F., Esposito, R., Marino, G., Costello, C.E., Velotta, R., and Birolo, L. (2013) Ultraviolet laser-induced cross-linking in peptides. Rapid. Commun. Mass Spectrom. 27, 1660-1668.

41) Stadtman, E.R., and Levine, R.L. (2003) Free radical-mediated oxidation of free amino acids and amino acid residues in proteins. Amino Acids. 25, 207-218.

42) Garrison, W.M., Jayko, M.E., and Bennett, W. (1962) Radiation-Induced Oxidation of Protein in Aqueous Solution. Radiat. Res. 16, 483-502.

43) Garrison, W.M. (1987) Reaction mechanisms in the Radiolysis of Peptides, Polypeptides, and Proteins. Chem. Rev. 87, 381-398.

44) Igarashi, N., Onoue, S., and Tsuda, Y. (2007) Photoreactivity of Amino Acids: Tryptophan-induced photochemical Events via Reactive Oxygen Species Generation. Anal. Sci. 23, 943-948.

45) Smith, K.C., Hodgkins, B., and O'leary, M.E. (1966) The biological importance of ultraviolet light induced DNA-protein crosslinks in Escherichia coli 15 TAU. BBA. 114, 1-15.

46) Saito, I., and Matsura, T. (1985) Chemical Aspects of UV-Induced Cross-Linking of Proteins to Nucleic Acids. Photoreactions with Lysine and Tryptophan. Acc. Chem. Res. 18, 134-141.

47) Greenberg, J.R. (1979) Ultraviolet light-induced crosslinking of mRNA to proteins. Nucleic Acids Res. 6, 715-732

48) Teale, F.W.J., and Weber, G. (1957) Ultraviolet Fluorescence of the Aromatic Amino Acids. Biochem J. 65, 476-482.

49) Husain, B., Mukerji, I., and Cole, J.L. (2012) Analysis of high affinity binding of PKR to dsRNA. Biochemistry. 51, 8764-8770.

50) Kauer, J.C., Erickson-Wiitanen, S., Wolfe Jr., H.R., and DeGrado, W.F. (1986) p-Benzoyl-L-phenylalanine, A New Photoreactive Amino Acid. J. Biol. Chem. 261, 10695-10700.

51) Chin, J.W., Martin, A.B., King, D.S., Wang, L., and Schultz, P.G. (2002) Addition of a photocrosslinking amino acid to the genetic code of Escherichia coli. Proc. Natl. Acad. Sci. USA. 99, 11020-11024.

52) Hino, N., Okazaki, Y., Kobayashi, T., Hayashi, A., Sakamoto, K., and Yokoyama, S. (2005) Protein photo-cross-linking in mammalian cells by site-specific incorporation of a photoreactive amino acid. Nature Methods. 2, 201-206.

53) Lee, H.S., Dimla, R.D., and Schultz, P.G. (2010) Protein-DNA photo-crosslinking with a genetically encoded benzophenone-containing amino acid. Bioorg. Med. Chem. Lett. 19, 5222-5224.

54) Dorman, G., and Prestwich, G.D. (1994) Benzophenone photophores in biochemistry. Biochemistry. 33, 5661-5673.

55) Lin, A.A., Sastri, V.R., Tesoro, G., and Reiser, A. (1988) On the Cross-linking Mechanism of Benzophenone-Containing Polymides. Macromolecules. 21, 1165-1169.

56) Wittelsberger, A., Mierke, D.F., and Rosenblatt, M. (2008) Mapping Ligand-receptor Interfaces: Approaching the Resolution Limit of Benzophenone-based Photoaffinity Scanning. Chem. Biol. Drug. Des. 71, 380-383.

57) Shields, C.J., Falvey, D.E., Schuster, G.B., Buchardt, O., and Nielson, P.E. (1987) Competitive Singlet-Singlet Energy Transfer and Electron Transfer Activation of Aryl Azides: Application to Photo-Crosslinking Experiments. J. Org. Chem. 53, 3501-3507.

58) Spanggord, R.J., and Beale, P.A. (2000) Selective Binding by the RNA Binding Domain of PKR Revealed by Affinity Cleavage. Biochemistry. 40, 4272-4280.

59) Bowie, A.G., and Unterholzne, L. (2008) Viral evasion and subversion of pattern-recognition receptor signaling. Nature Reviews Immunology. 8, 911-922.

Figures

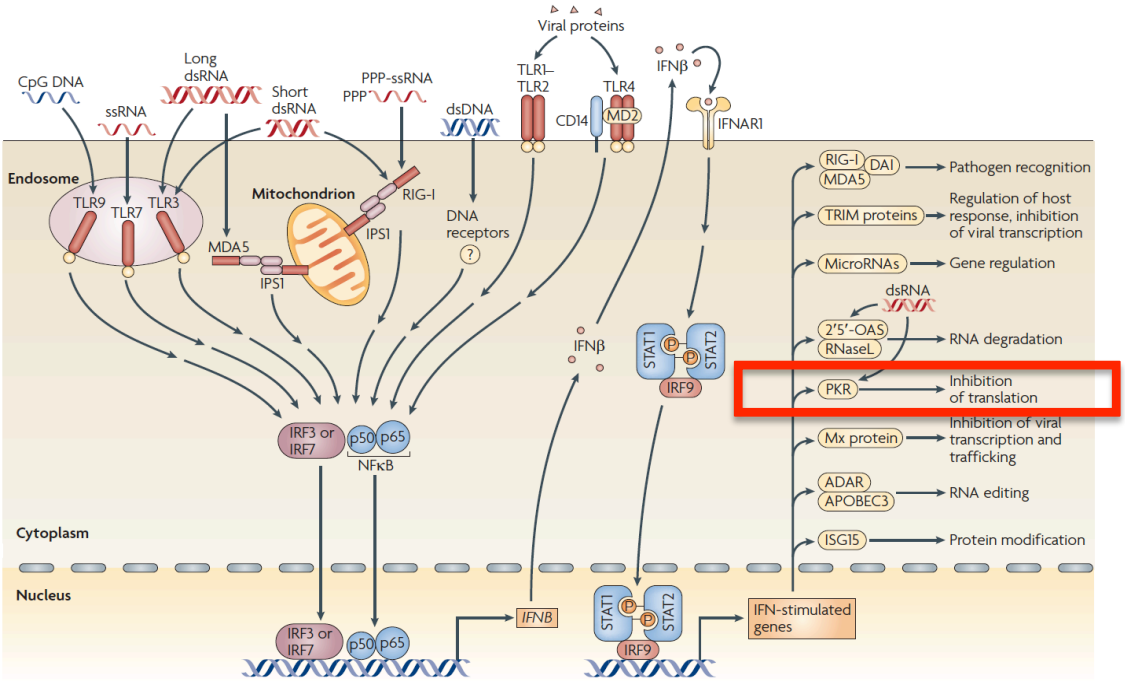

Figure 1. PKR is Involved in the Intracellular Innate Immune Response (59). PKR is one component in the innate immune response and is indicated here in red. The protein is induced by interferon in a latent state and is activated upon binding to dsRNA.

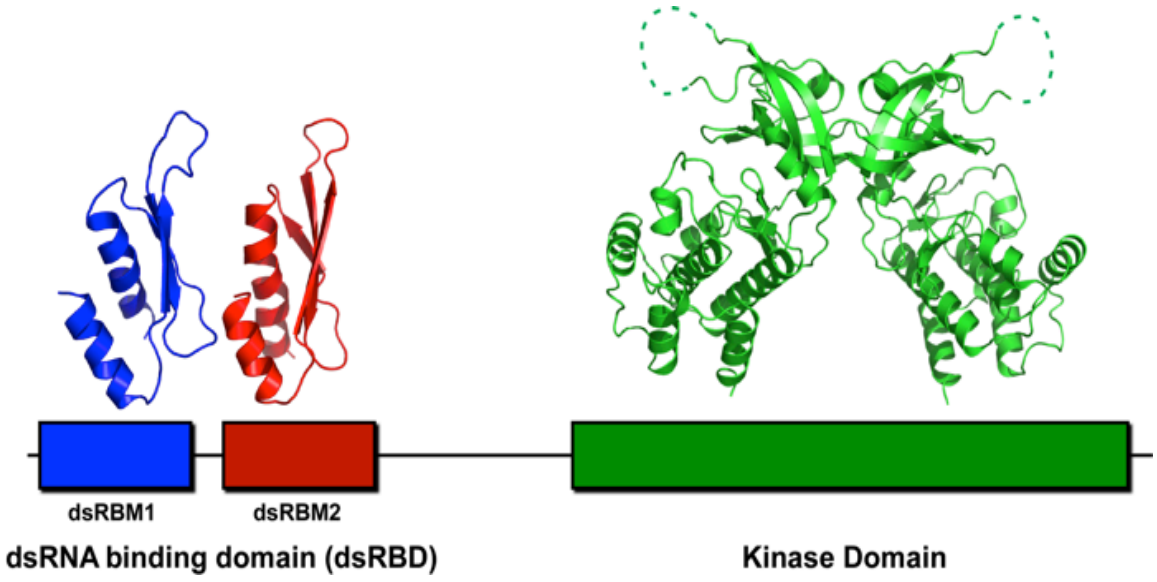

Figure 2. PKR Structures.
PKR consists of an N-terminal dsRNA binding domain (dsRBD) and a C-terminal kinase domain connected by a ~90 residue linker. The dsRBD is comprised of two tandem dsRBMs both with a conserved αββββα fold.

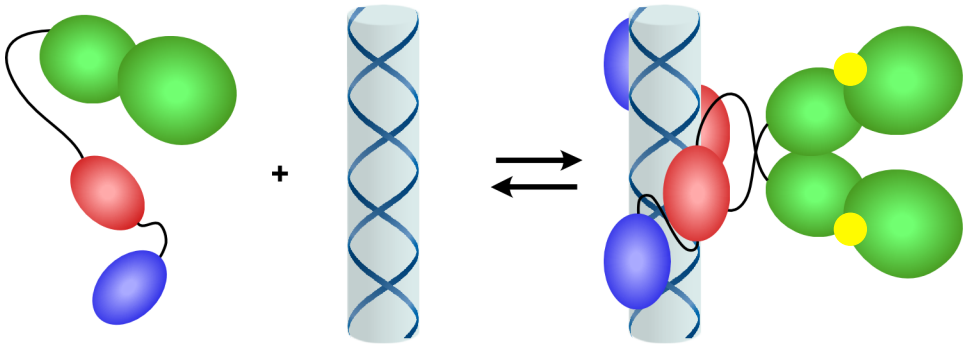

Figure 3. PKR Activation and Dimerization Model
Upon binding to dsRNA, two PKR monomers dimerize on the duplex RNA and induce activation of the dimer by autophosphorylation at the kinase domain shown here in yellow

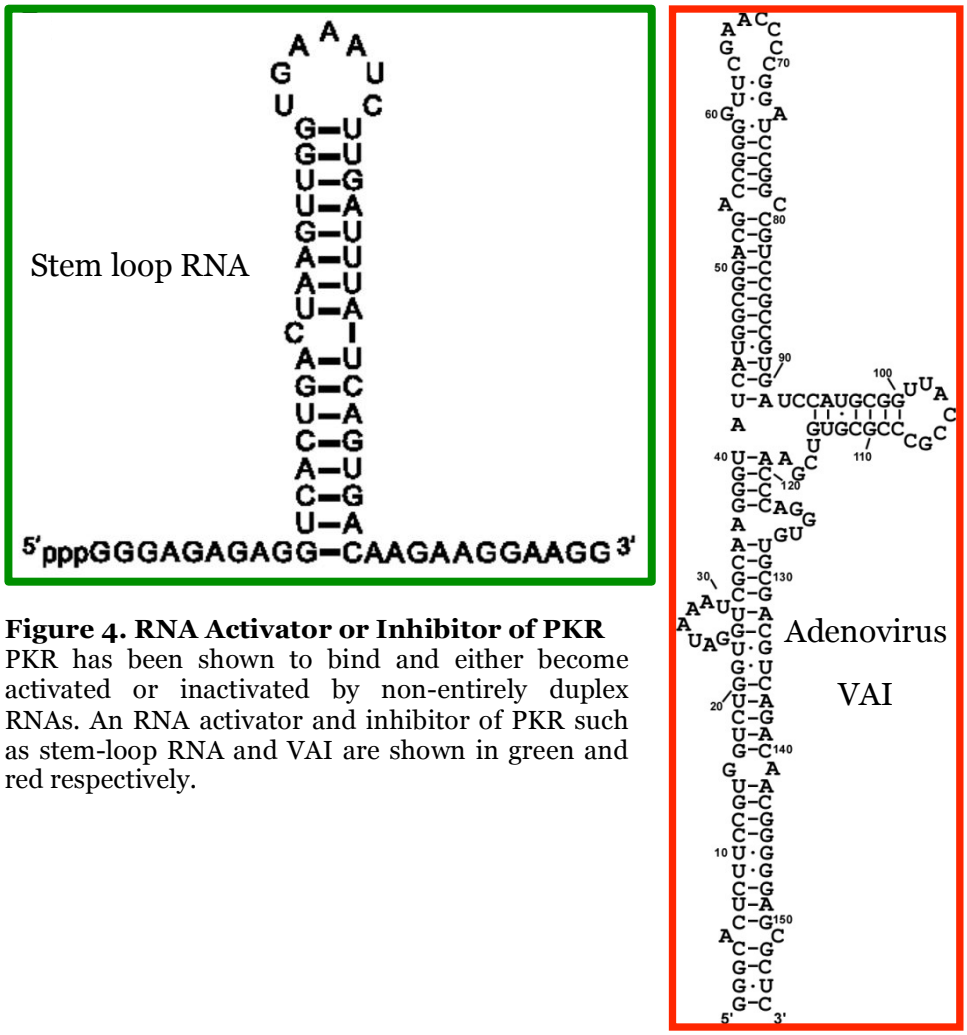

Figure 4. RNA Activator or Inhibitor of PKR
PKR has been shown to bind and either become activated or inactivated by non-entirely duplex RNAs. An RNA activator and inhibitor of PKR such as stem-loop RNA and VAI are shown in green and red respectively.

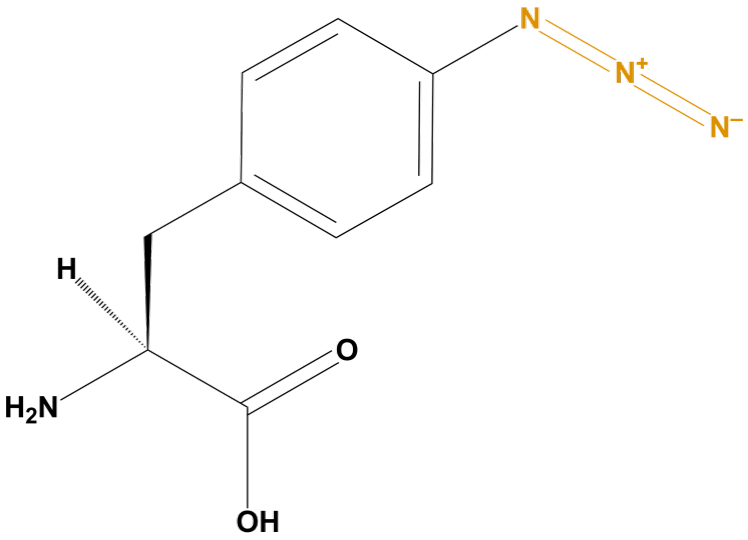

Figure 5. The Unnatural Amino Acid: *p-azido-l-phenylalanine*
The azide region of the amino acid involved in the crosslinking reaction is denoted in orange.

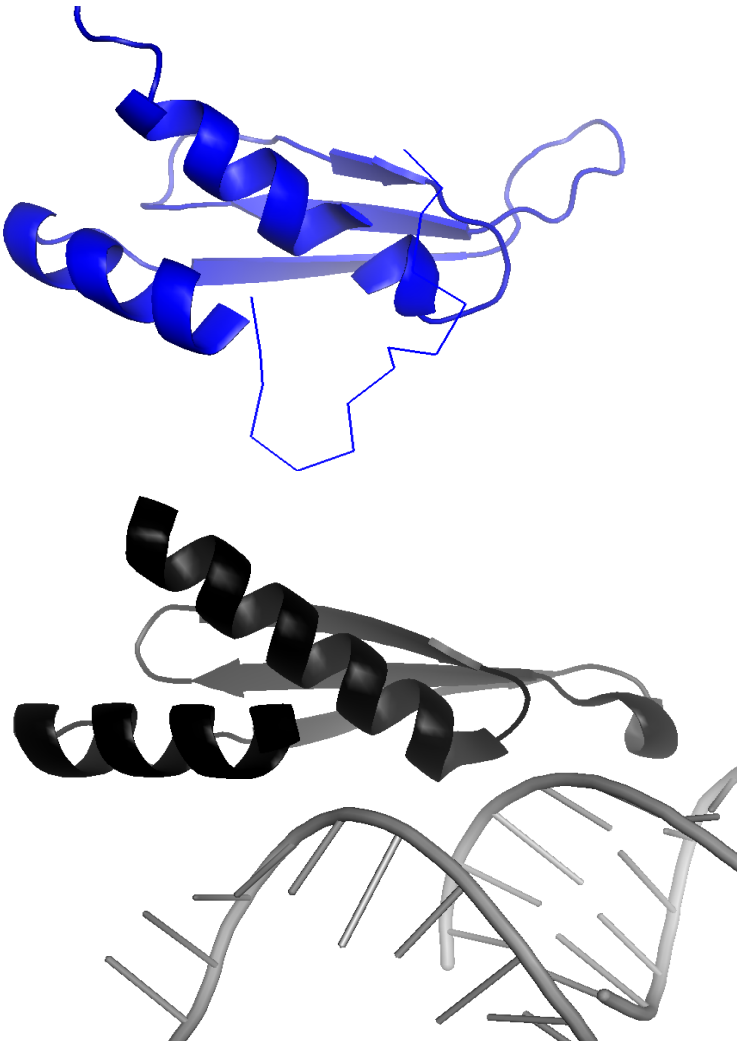

Figure 6. Structure of PKR's dsRBM1 and Xlrbpa-2 Complexed with dsRNA
There is an available solution crystal structure of PKR's dsRBM1 and Xlrbpa complexed with dsRNA. Both are shown here in blue and black respectively.

Figure 7. PKR's dsRBM1 Overlaid with Xlrbpa Bound to dsRNA
F43, F9, E29, D38, N65, and R39 are the candidate residues shown in green, pink, red, orange, purple, and light blue respectively.

F9pAzF
Forward Primer—5'-TCTTTCAGCAGGT***TAG***TTCATGGAGGAACTTAATACATAC-3'
Reverse Primer—5'-GTTCCTCCATGAA***CTA***ACCTGCTGAAAGATCACCAGCCAT-3'

E29pAzF
Forward Primer—5'-ACTTAAATATCAA***TAG***CTGCCTAATTCAGGACCTCCACATGATA-3'
Reverse Primer—5'-CTGAATTAGGCAG***CTA***TTGATATTTAAGTACTACTCCCTGCTTCT

D38pAzF
Forward Primer—5'-AGGACCTCCACAT***TAG***AGGAGGTTTACATTTCAAGTT
Reverse Primer—3'- ATGTAAACCTCCT***CTA***ATGTGGAGGTCCTGAATTAGGCAG

F43pAzF
Forward Primer—5'-TAGGAGGTTTACA***TAG***CAAGTTATAATAGATGGAAGAGAA-3'
Reverse Primer—5'-CTATTATAACTTG***CCTA***GTAAACCTCCTATCATGTGG

N65pAzF
Forward Primer—5'-AGGACCTCCACAT***TAG***AGGAGGTTTACATTTCAAGTT
Reverse Primer—3'- ATGTAAACCTCCT***CTA***ATGTGGAGGTCCTGAATTAGGCAG

R39pAzF
Forward Primer—5'-ACCTCCACATGAT***TAG***AGGTTTACATTTCAAGTT-3'
Reverse Primer—5'-GAAATGTAAACCT***CTA***ATCATGTGGAGGTCCTGAATTAGG

Figure 8. Primer Design
Above are the sequences of the primers used in the site-directed mutagenesis for the creation of each PKR plasmid construct.

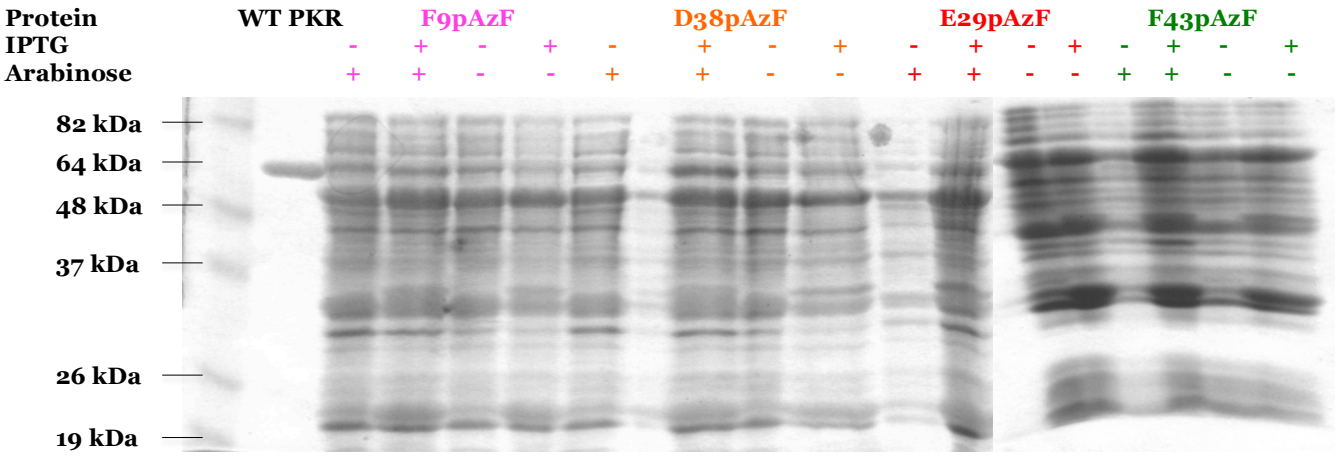

Figure 9. PKR Construct Induction I
Shown above are the cell lysates of transformed Arctic Express cells containing their respective PKR construct. The cells were induced with IPTG (+) and Arabinose(+) to induce gene expression of the PKR construct and of the aminoacyl-tRNA synthetase pair respectively.

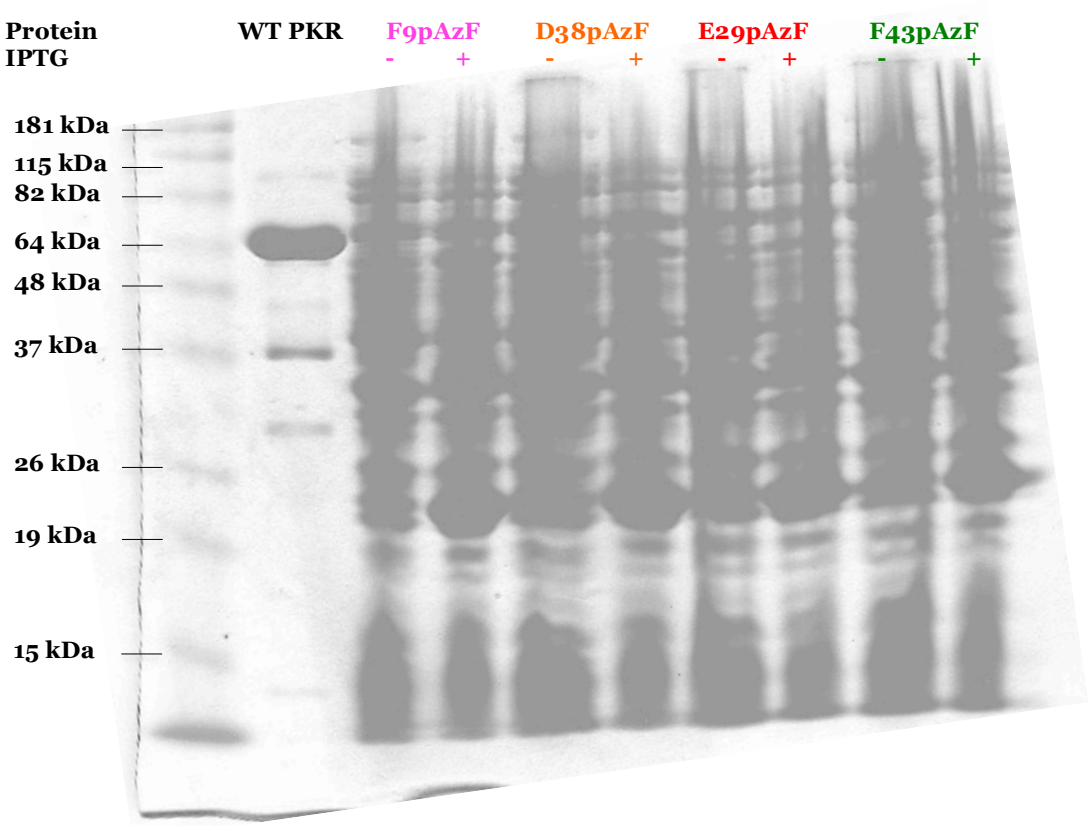

Figure 10. PKR Construct Induction II
Shown above are the cell lysates of transformed Arctic Express cells containing their respective PKR construct. The cells were induced with IPTG to induce gene expression of the PKR construct.

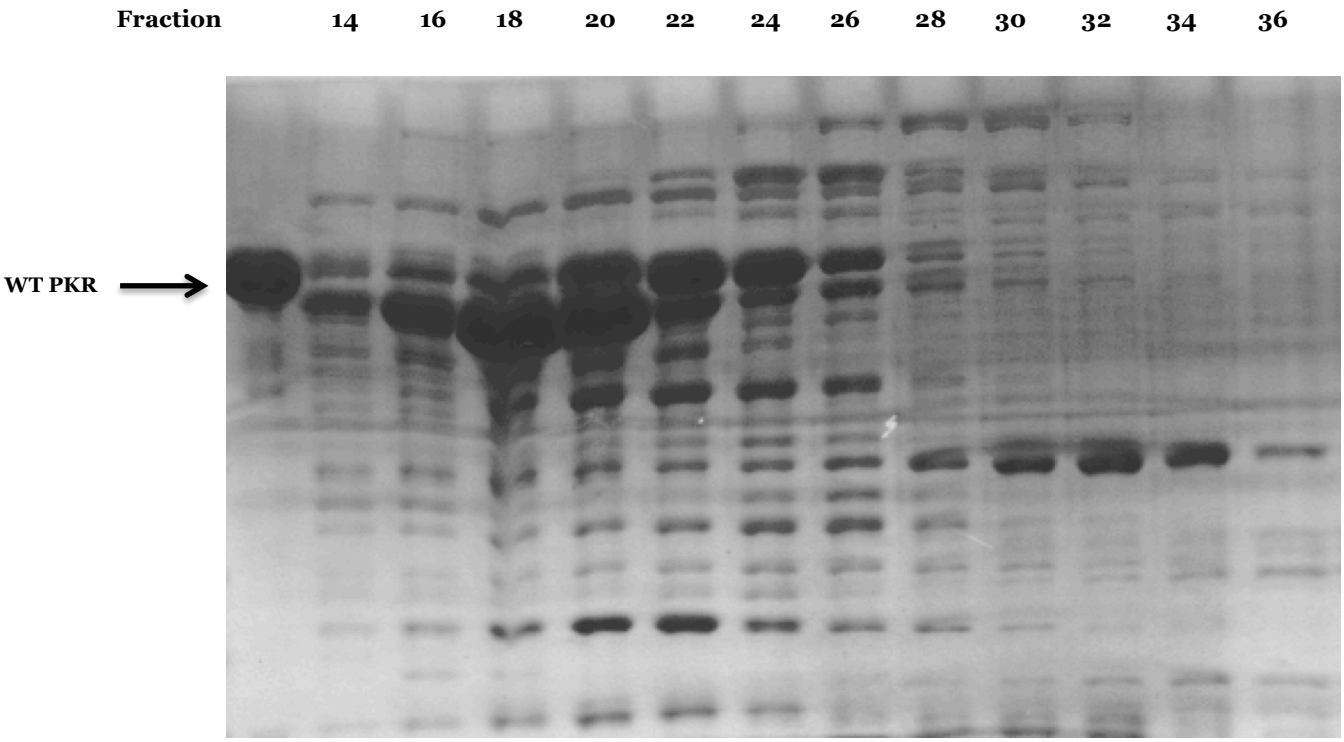

Figure 11. F43pAzF Heparin Column Gel Fractions

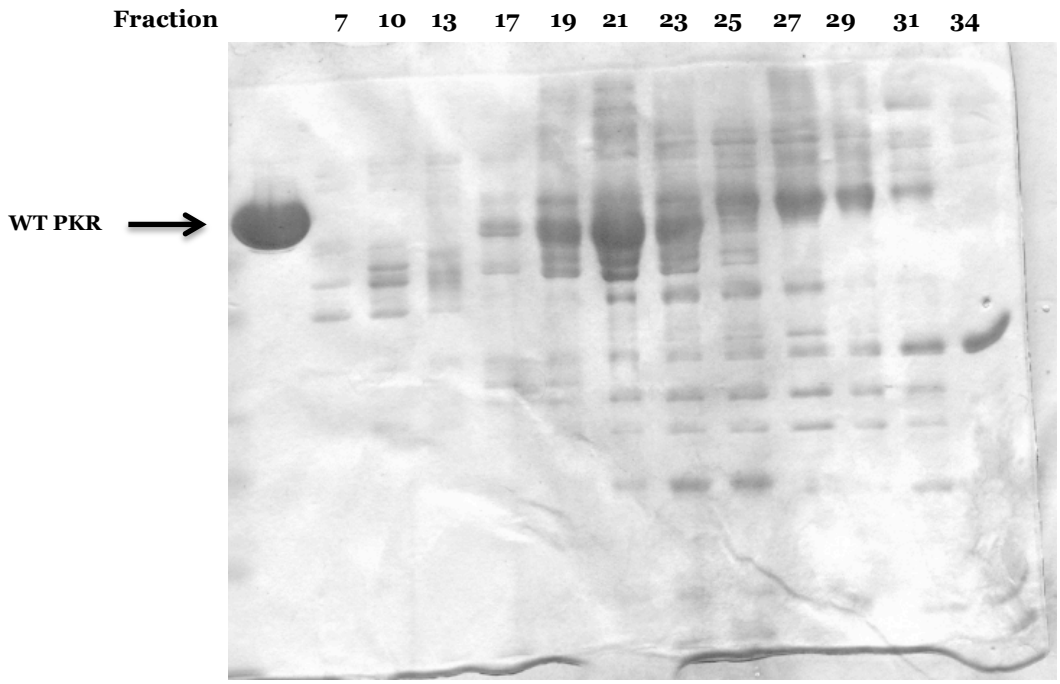

Figure 12. D38pAzF Heparin Column Gel Fractions

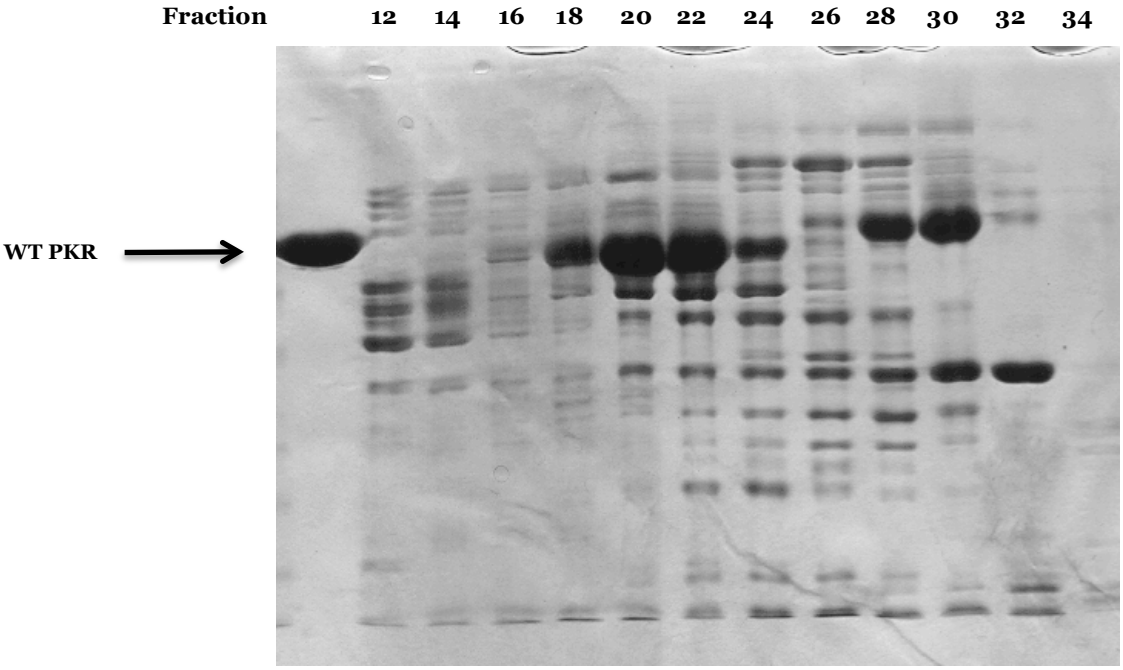

Figure 13. E29pAzF Heparin Column Gel Fractions

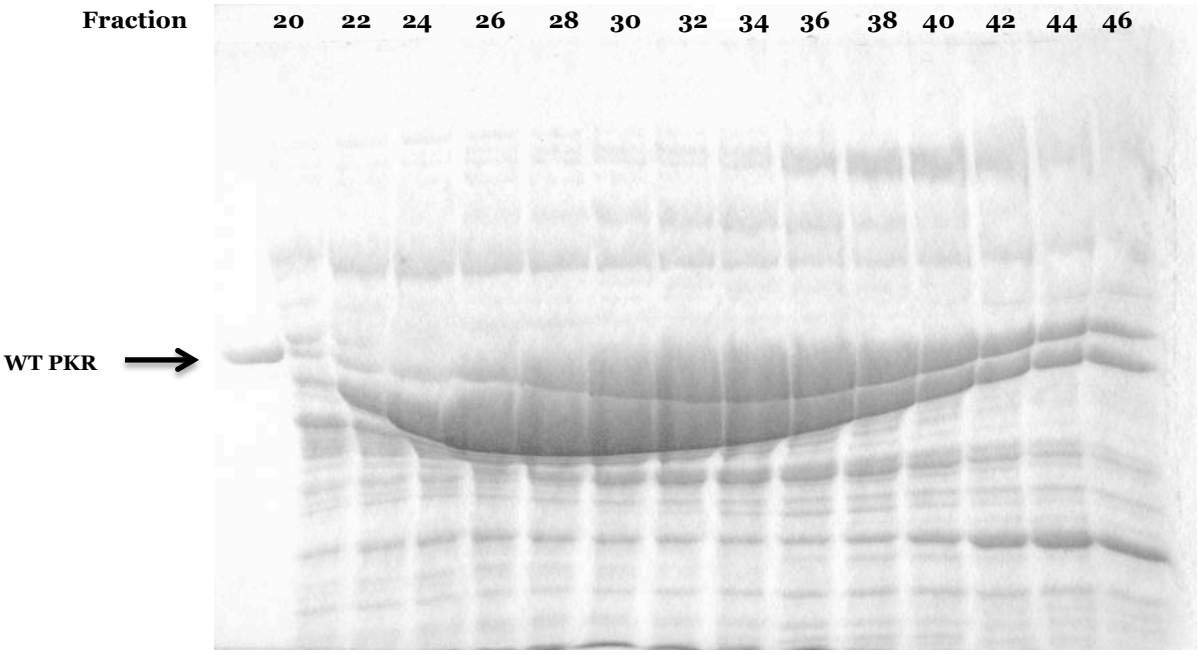

Figure 14. F9pAzF Heparin Column Gel Fractions

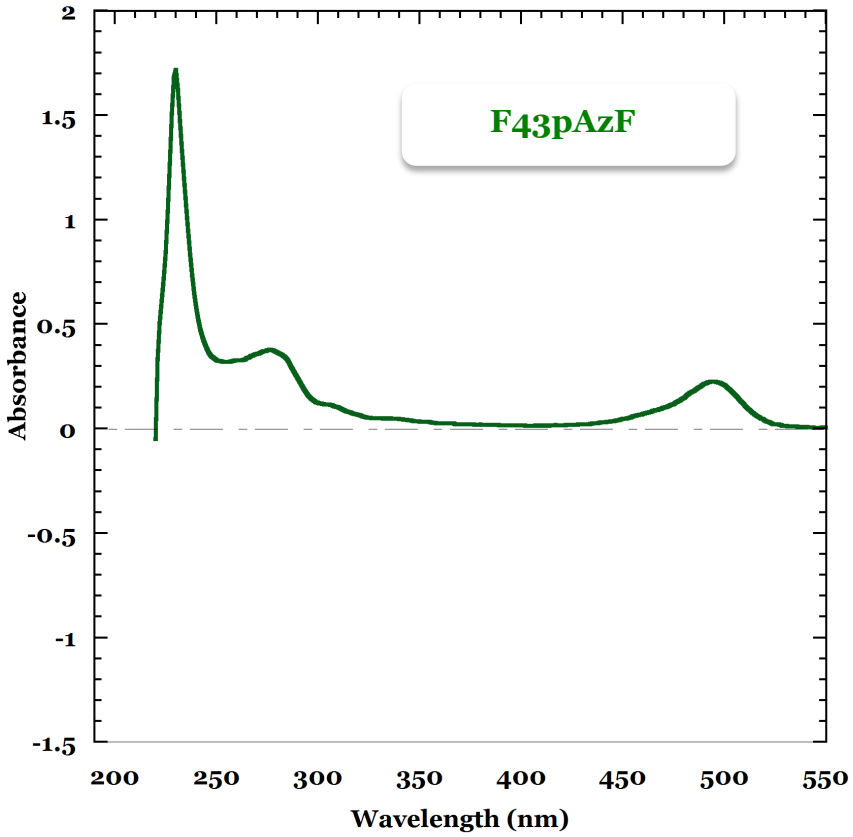

Figure 15. Absorption Spectra of Labeled F43pAzF

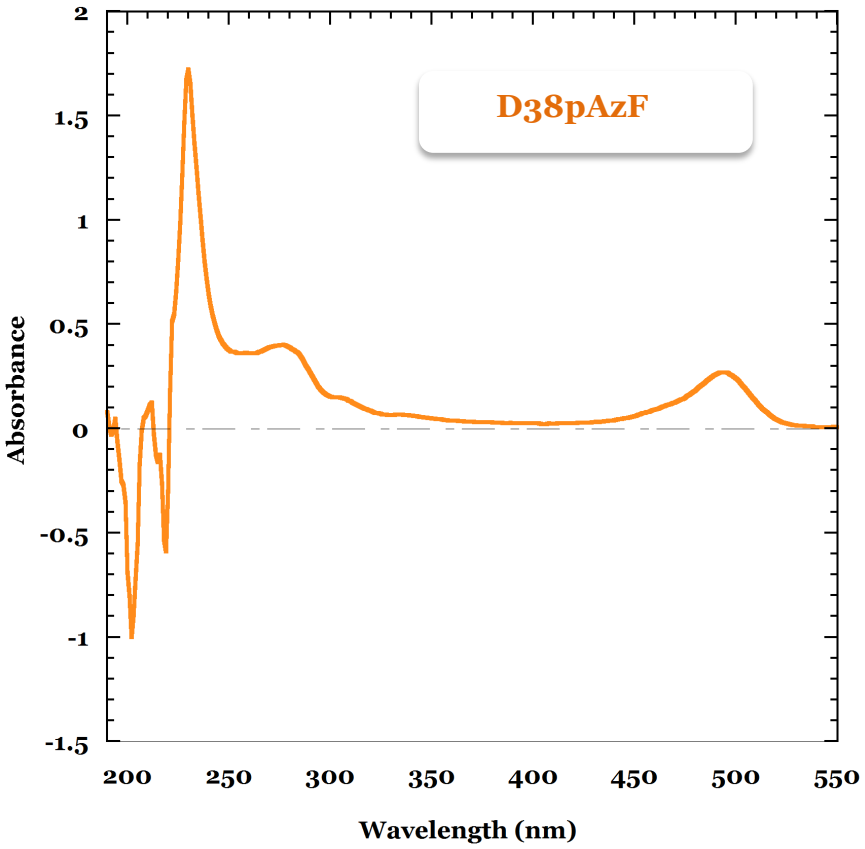

Figure 16. Absorption Spectra of Labeled D38pAzF

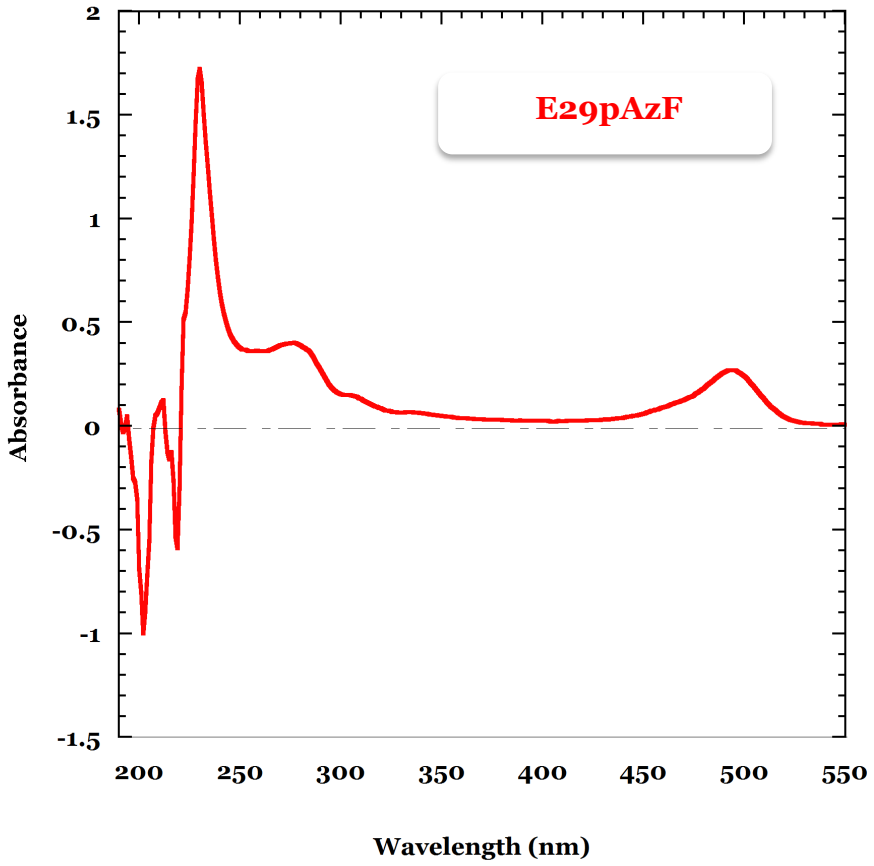

Figure 17. Absorption Spectra of Labeled E29pAzF

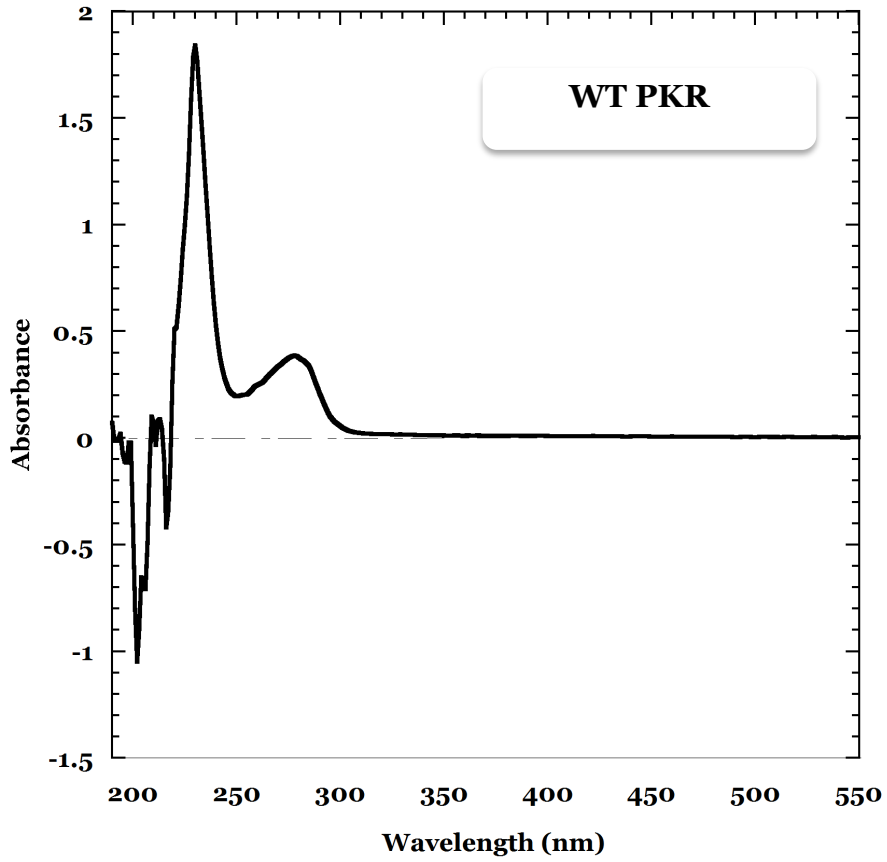

Figure 18. Absorption Spectra of Unlabeled WT PKR

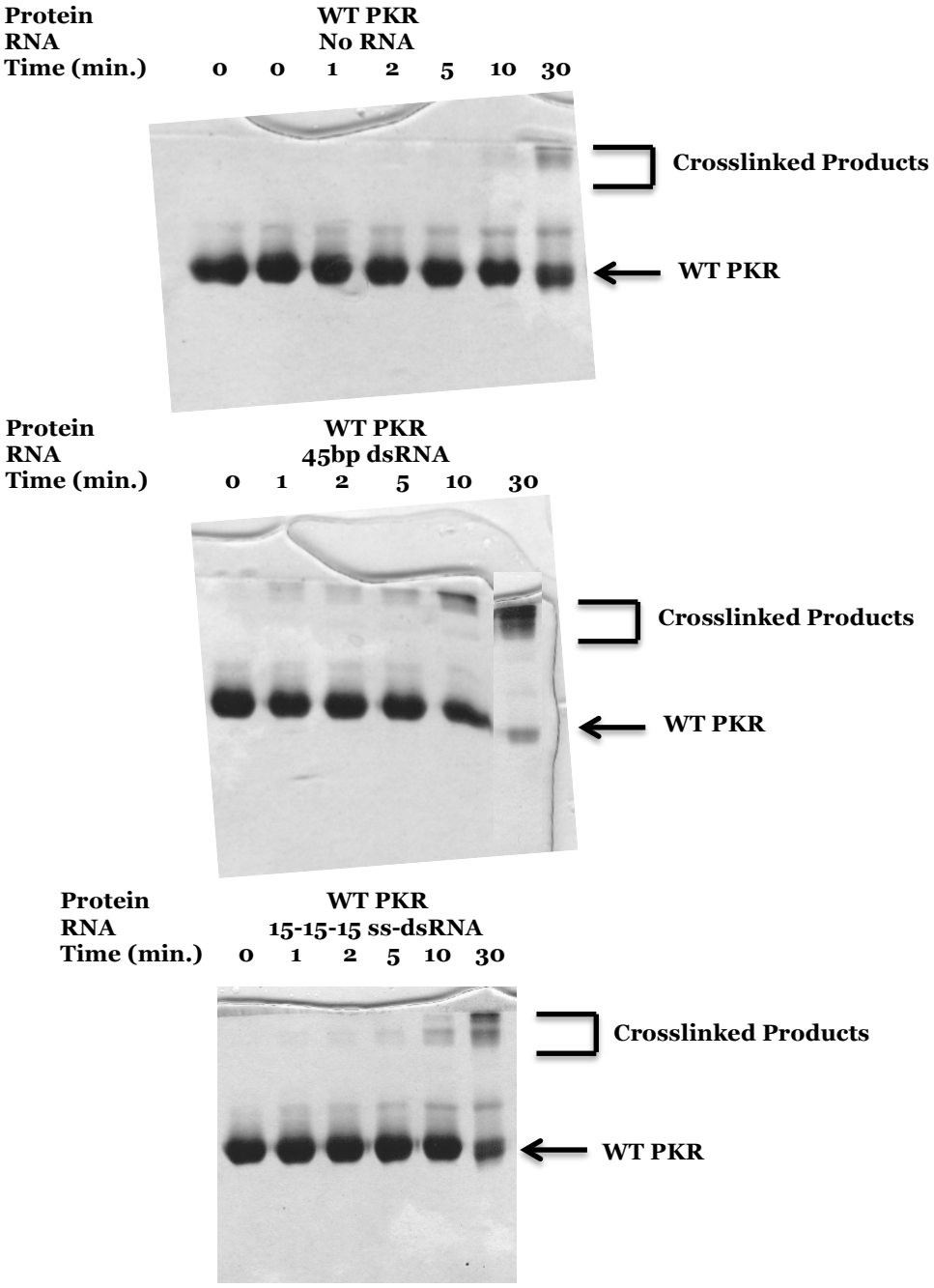

Figure 19. Crosslinking of WT PKR with RNA at 302nm

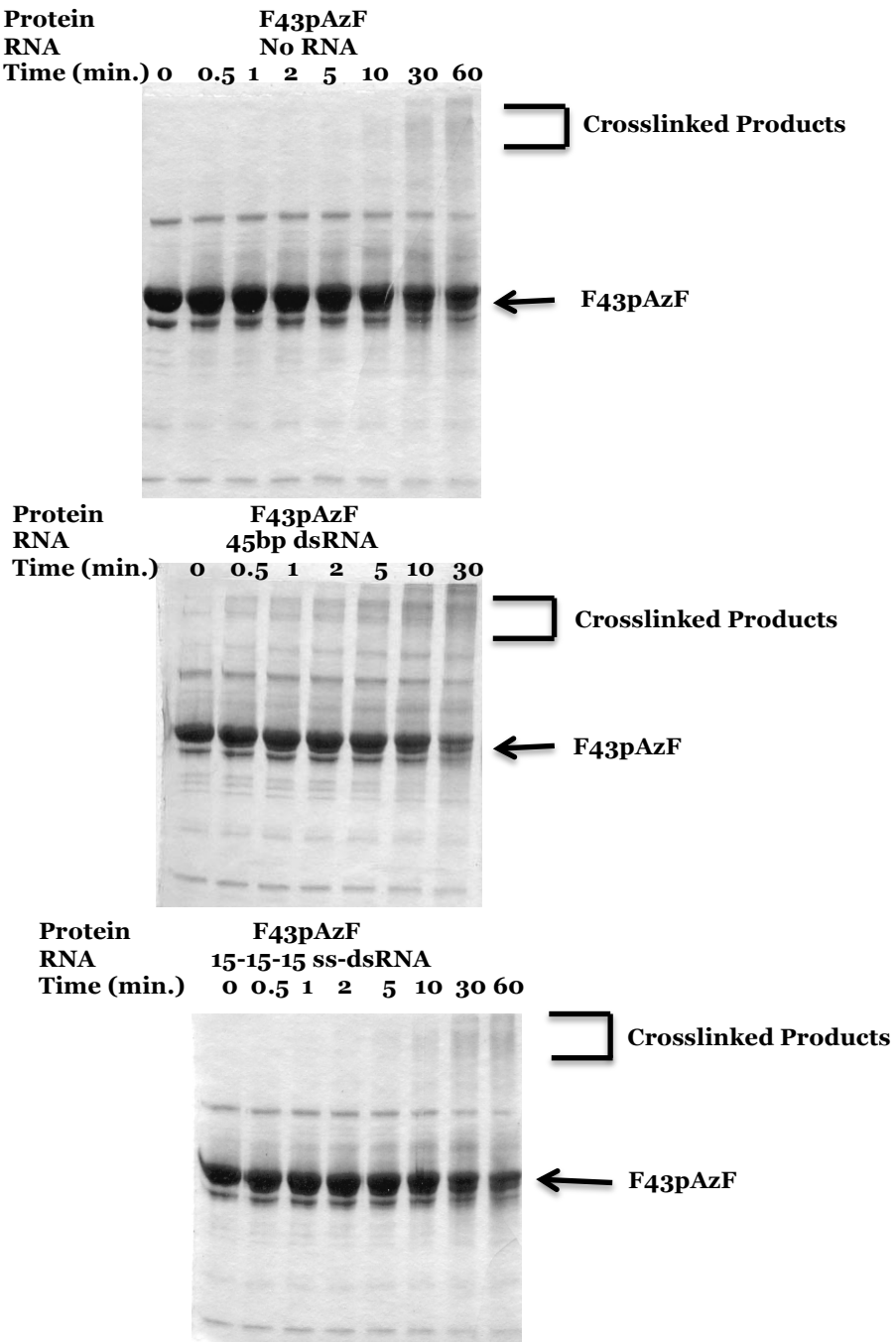

Figure 20. Crosslinking of F43pAzF with RNA at 254nm

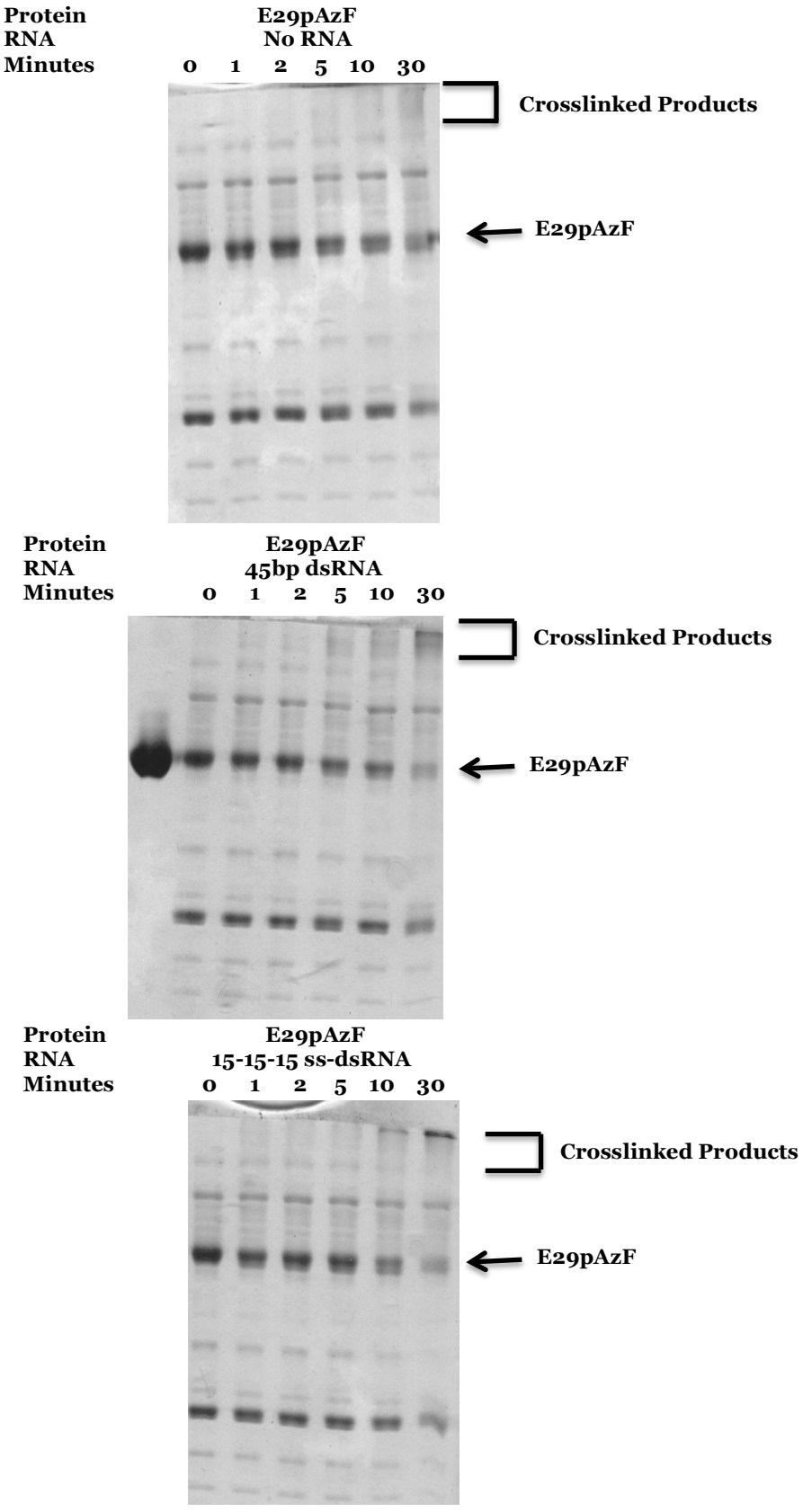

Figure 21. Crosslinking of E29pAzF with RNA at 302nm

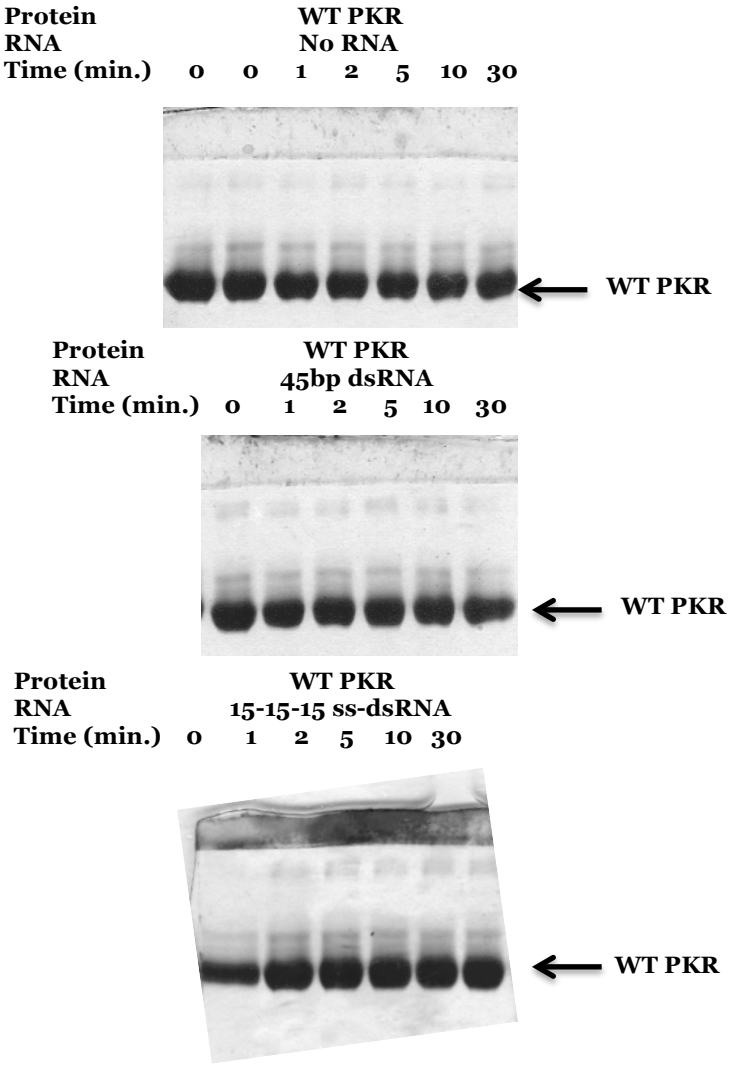

Figure 22. Crosslinking of WT PKR with RNA at 365nm

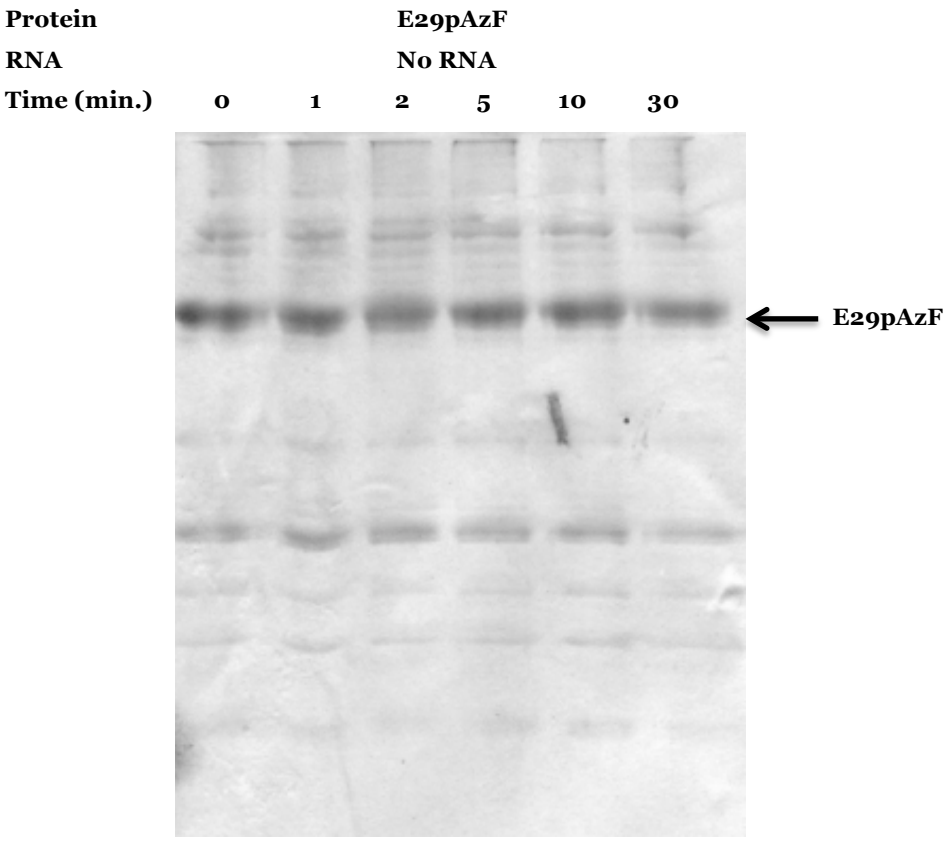

Figure 23. Crosslinking of E29pAzF in the Absence of RNA at 365nm

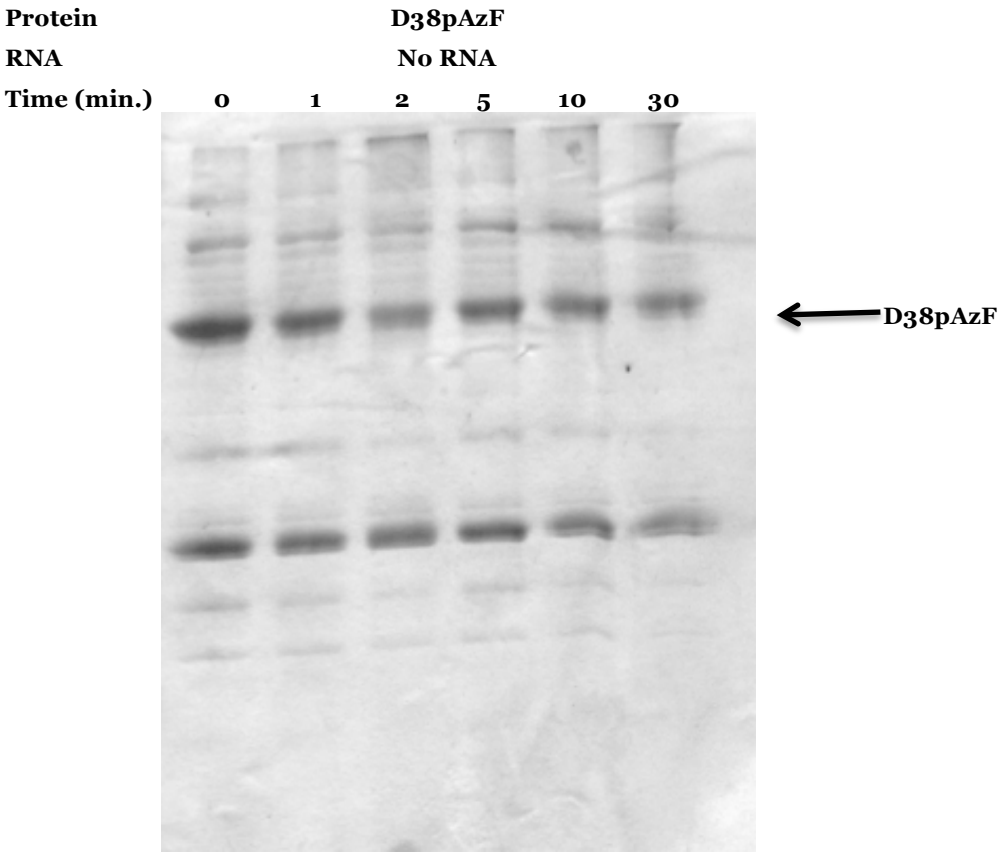

Figure 24. Crosslinking of D38pAzF in the Absence of RNA at 365nm

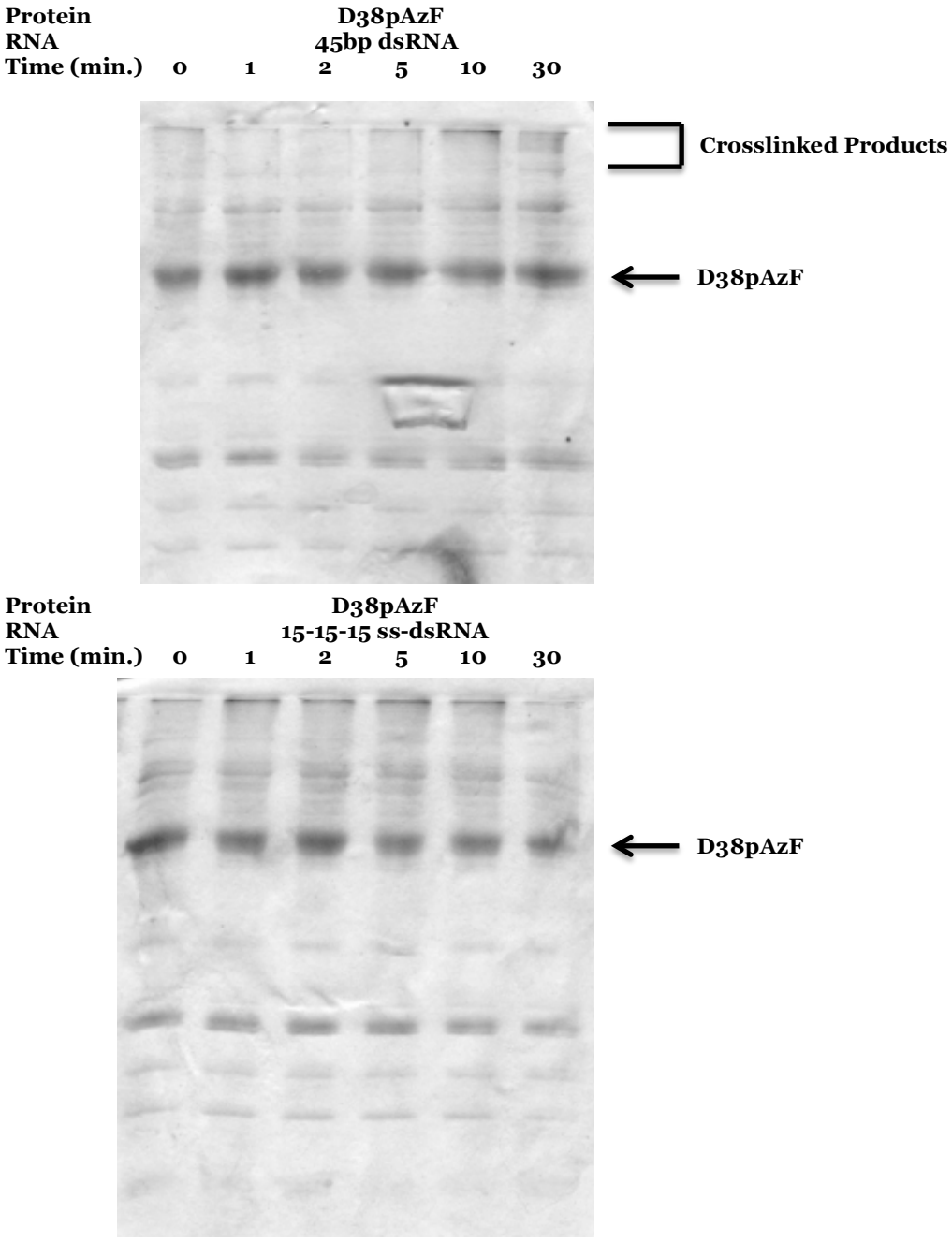

Figure 25. Crosslinking of D38pAzF with RNA at 365nm

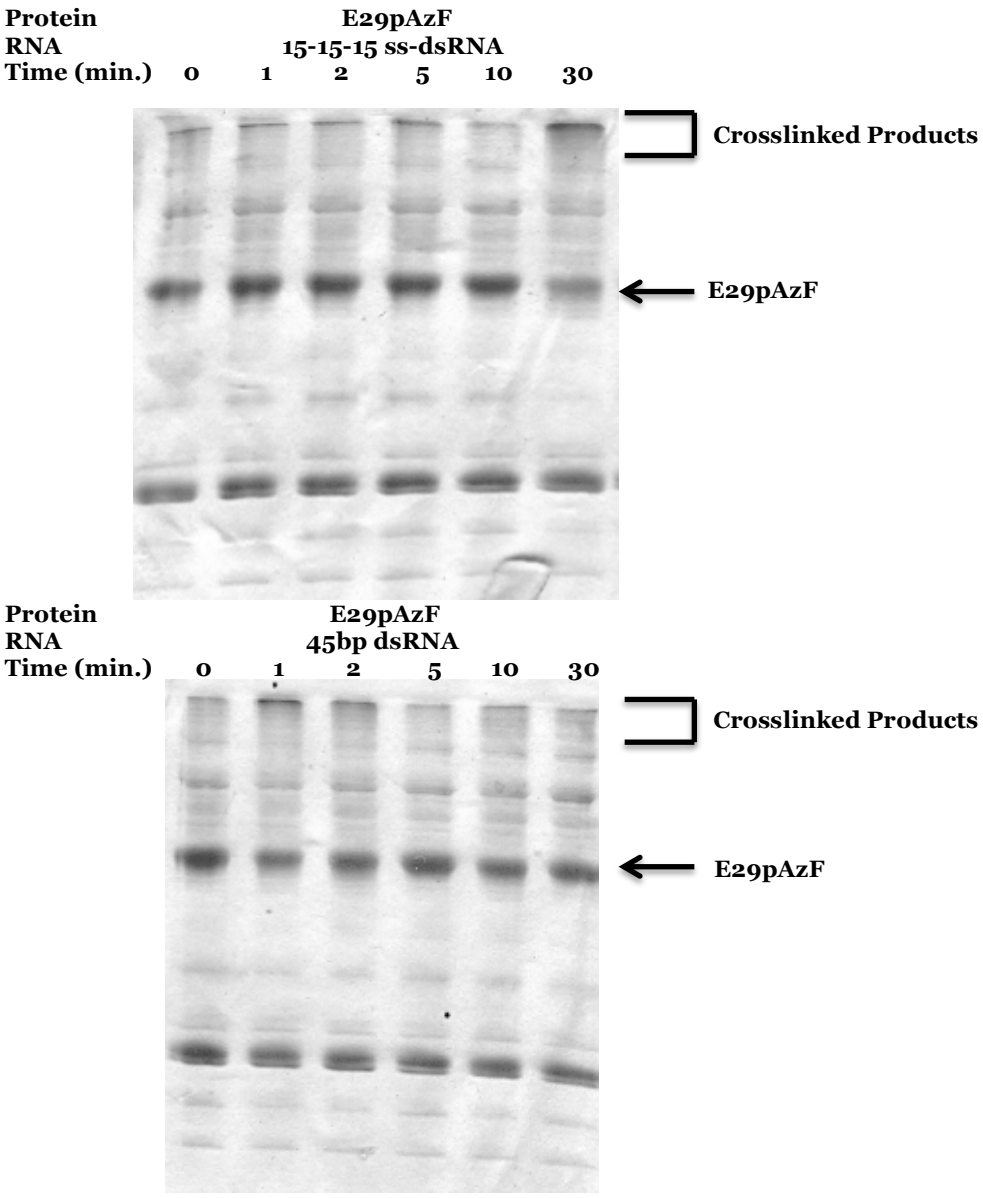

Figure 26. Crosslinking of E29pAzF with RNA at 365nm